FACULDADE DE ENGENHARIA DA UNIVERSIDADE DO PORTO

Enhancing Wave Energy Converter with Control Algorithms driven by Artificial Intelligence

João Eduardo Gomes Alves

Mestrado em Engenharia Eletrotécnica e de Computadores

Supervisor: Aníbal Castilho Coimbra de Matos

Co-Supervisor: Nelson Daniel Ferreira Gonçalves

November 27, 2022

Abstract

Ocean energy is a significant renewable energy source that, if correctly exploited, can have a surprising contribution to the global energy demands, especially to countries with seacoast exposure. It is still in a development phase, and one of the most promising and developed systems is the Oscillating water column (OWC). Since this type of system still can't compete with others types of renewable energy due to its cost and efficiency, optimising the Power take-off (PTO) of this type of system can be valuable.

Two approaches to control the PTO were made: PID Controller tuned using a Particle swarm optimization (PSO) algorithm and an Artificial Neural Network (ANN) with a PSO algorithm that finds the optimal generator control parameter. Both control approaches were compared against a simple control rule which uses fixed generator control parameters in order to check if the overall efficiency of the system is enhanced.

Both approaches lead to a higher energy capture efficiency in relation to the simple reference control rule. It should be noted that the control approach, which uses the ANN, had a better performance, especially in the lower energetic sea states. Using a PID controller made the generator act as a motor, consuming energy from the grid when the control law wants to increase the turbine rotational speed. A generator overload protection and high-speed safety valve are also used to protect the OWC system and prevent damage.

Although both approaches seem to be promising, both were done considering perfect conditions, like an instantaneous valve closure, the sea states used to make control decisions were known instead of predicted, and the study uses a fully trained ANN instead of incrementally training the ANN with the collected data along the time.

Resumo

Energia oceânica é uma das fonte de energia renovável mais significantes, em que se corretamente exploradas, consegue trazer uma contribuição surpreendente para as exigências energéticas globais. Ainda está numa fase de desenvolvimento, onde um do sistemas mais promissores e desenvolvidos é o *Oscillating water column* (OWC). Já que este tipo de sistema ainda não consegue competir com outros tipos de energia renovável, devido ao seu custo e eficiência, otimizar o sistema de retiro de potencia pode ser importante.

Foram realizadas duas abordagens para controlar a potencia retirada: controlador PID tunado a partir de um algoritmo *Particle swarm optimization* (PSO) e uma ANN com um algoritmo PSO que encontra os parâmetros ótimos de controlo do gerador. Ambos estes métodos de controlo foram comparados com uma simples regra de controlo, que usava um parâmetro fixo de controlo do gerador, para verificar se a eficiência no geral aumentava.

Ambas as abordagens aumentaram a eficiência de captura energética em relação à simples regra de controlo. È de notar que a abordagem que usa a ANN teve um melhor desempenho, especialmente em estados do mar menos energéticos. O uso do controlador PID fez com que o gerador tenha agido como um motor, consumindo energia da rede nas alturas que a lei de controlo queria aumentar a velocidade de rotação da turbina. Um controlo que protege o gerador de entrar em sobrecarga também é usado, e uma *high-speed safety valve* também é usada para proteger o OWC e evitar danos.

Apesar de ambas as abordagens parecem promissoras, ambas foram feitas considerando condições perfeitas, tal como a válvula de proteção fechar instantaneamente, os estados do mar para fazer as decisões de controlo era previamente conhecidas em vez de previstas, e o estudo usou uma ANN totalmente treinada, em vez de um treino incremental desta, com dados recolhidos ao longo do tempo.

Acknowledgement

First of all, many names won't be mentioned since I wouldn't be able to thank each and everyone that shared this academic journey with me.

To my supervisor, thank you for allowing me to develop this thesis and for the help given. To my co-supervisor, thank you for all the time invested in helping this thesis development, enabling me to work on this theme, and for always being available to help.

To my family, thank you for all the advice given to me throughout these years, for making me the person I am today, for always believing in me, and being my role model.

To my friends, thank you for making me realise even in the toughest times, I still should find time to crack a smile and relax.

" The time you enjoy wasting is not wasted time "

- Bertrand Russell

Contents

List of Figures

List of Tables

Abbreviations

AI	Artificial intelligence
ANN	Artificial neural network
BEP	Best efficiency point
BBDB	Backward bent-duct buoy
DFIG	Double-fed induction generator
FBDB	Foward bent-duct buoy
FLC	Fuzzy logic controller
GSC	Grid side converter
HSSV	High speed safety valve
IAE	Integral of absolute error
MAE	Mean absolute error
MPPT	Maximum power point tracking
OWC	Oscillating water column
PLC	Programmable logic controller
P_s	Active Power
PSO	Particle swarm optimisation
PTO	Power Take-off
OPC	Optimised Parameters Control
RPM	Rotations per minute
R_s	Reactive Power
RSC	Rotor side converter
ReLU	Rectified linear activation unit
WEC	Wave Energy Converter

Symbols

a	Generator control law constant
A^{∞}	Added mass at infinite
b	Generator control law exponent
D	Rotor diameter
D_w	Wavelength
F_d	Excitation force
f_o	Frequency of occurrence
F_w	Wave energy force
g	Gravity acceleration
Hs	Significant wave height
I	Inertia
m	Mass of the water displaced by the OWC chamber
m_c	Instantaneous mass inside the air chamber
$\dot{m_{turb}}$	Mass flow rate of air through the air turbine
p^*	Dimensionless relative pressure oscillation inside the chamber
P_{ctrl}	Instantaneous generator electromagnetic power imposed to control the rotational speed
Pg_{avg}	Average generated power
P_{gen}^{rated}	Generator rated power
$\overline{P_{OWC}}$	the average potency
P_{turb}	Instantaneous turbine aerodynamic power
P_w	Wave energy power
R	Radiation Force
S	Cross-sectional chamber area
T_{ctrl}	Controlled electromagnetic torque
T_d	Derivative time
Te	Wave energy Period
T_{gen}^{max}	Maximum allowed torque
T_i	Integrative time
T_t	Tracking time constant
v	Instantaneous velocity of the imaginary cross section between the air the the water level in the chamber
V_c	Air chamber volume
V_0	Air volume inside the chamber in calm water
v_w	Wave velocity
z	Instantaneous position of the imaginary cross-section between the air and the water level in the chamber
ρ_c	Air density inside the air chamber
ρ_{at}	Air density in atmospheric conditions

η	Efficiency
Δp	Stagnation pressure head between the air chamber and the atmosphere
γ	Specific heat ratio
Ω	Turbine rotational speed
Ω_{ctrl}^{max}	Rotational speed limit
ω_{gen}^{nom}	Nominal angular speed where the generator is at its rated power
Ω_{gen}^{nom}	Nominal rotational speed where the generator is at its rated power
ϕ	Turbine dimensionless flow rate
π	Turbine dimensionless power coefficient
Ψ	Turbine dimensionless pressure head
ρ_{in}	Turbine inlet density at stagnation conditions
ρ_w	Water density

Chapter 1

Introduction

Lately, renewable energy has been a growing interest since the excessive usage of limited fossil fuels has been deteriorating the environment [8]. Hence, in the last decade, the interest in renewable energy, such as wind, solar, hydro, and biomass, has risen rapidly and with economic success in some cases.

Currently, one of the most unexploited energy sources is oceanic energy, but it's still at an early stage of development [9]. However, if this technology is extensively refined, it may be able to supply enough energy to support countries that have their coast facing the ocean [5].

Oceanic energy can be decomposed in two main types:

- tidal energy
- wave energy

Both energy types are way less unpredictable to when and how these resources are available than other renewable energy sources. Between tidal and wave energy, wave energy has a lower variability in short time spans [9], is a continuous energy source contrary to tidal and has a lower environmental impact.

Highlighting wave energy, a wide variety of concepts were developed to take advantage of it. Each WEC (Wave Energy Converter) can be classified using two main categories: location and type. However, this classification can be further specialised when assuming their mode of operation, leading to three main devices:

- Oscillating bodies
- Oscillating water column (OWC)
- Overtopping device

This work will focus on the enchanting strategies of an OWC (Oscillating water column) system since it has one of the biggest potentials among WECs, with satisfactory performance and a low environmental impact. This type of system also has high reliability since the moving

mechanical parts aren't under seawater, it's easy to maintain, uses sea space efficiently, and can be adapted to different locations [10, 11].

This system can be divided into two different sub systems: air chamber and the Power take-off (PTO). This PTO consists of turbine/generator set, where the turbine has to be a self-rectifying air turbines, since it allows the bidirectional air flow caused by the compressed and decompressed air inside the chamber cause by the OWC water level variation. There are two main types of turbines: Wells and Impulse turbines, where the latter one has a wider operation range, considering the allowed airflow inside the turbine, but has a lower peak efficiency. Therefore, the chosen turbine type has to take into account most common airflow value, and if it tends to vary in a wide range of values.

A major point in improving the overall OWC efficiency is how the PTO is controlled. Therefore this type of control can be divided into two main types: stalling prevention and latching control. This work focus on the stalling prevention, resulting in two different approaches:

- Optimal turbine parameters control
- PID turbine control

Both these methods were studied in order to infer the viability of their use, and different advantages of each one.

The following document is organised under the following heading: Chapter 2 gives an insight of the different development status and available wave technologies. Chapter 3 gives information on the study's methodology. Chapter 4 explains how the equations behind the OWC model are interlinked. Chapter 5 shows the procedure of the study and what will be studied. Chapters 6 and 7 show the different results of the case study and its discussion. Finally in the Chapter 8, conclusions and a proposal of a future work is made.

Chapter 2

Background

In this chapter, a review and clarification of the different concepts and themes are made. Its main objective is to provide the reader with fundamental knowledge about the state of development, models, and application of the chosen technology.

2.1 Ocean Energy Converter

As mentioned before, the increased energy demand and the excessive usage of limited fossil fuels are the main factors in the increased interest in ocean energy converter technologies [12].

Ocean energy can be divided into five main categories: ocean wave, tidal range, tidal current, ocean thermal energy, and salinity gradient. However, most of these types of energy aren't developed near enough, being merely at a conceptual and demonstration stage, except for tidal current and wave energy [9].

This Section will have a brief discussion comparing the two main types of ocean energy (wave and tidal current energy), highlighting their potential.

2.1.1 Tidal current

The rise and fall of sea levels induced by the gravitational pull of the moon and sun on the Earth generate tidal energy. This type of energy, relatively to classic renewable energy, has a clear advantage of being way more predictable [13]. The tides' regularity and an enormous amount of energy potential make tidal energy development appealing [12].

This type of energy has a clear advantage compared to a classic hydroelectric power station because a tidal barrage allows water to flow in both ways, even though it usually captures its energy from a high to low tide [12]. A clear disadvantage is that this type of energy relies highly on its geographical location.

2.1.1.1 Potential

Studies estimated that 500-1000 TWh/y are available worldwide, and only accounting for the inlet of Ria de Aveiro, 199 GWh/y could be produced [14]. However, today economic and environmental restrictions only allow a portion of this energy potential to be exploited.

As mentioned before, this type of energy is highly dependent on the site, in other words, where each device is allocated since its capture can be enhanced by reflections of large peninsulas or resonant effects produced by the magnitude of the tidal wave [12].

2.1.2 Wave Energy

Waves form as the wind blows over water, resulting from the temperature and pressure variations throughout the world. These waves carry kinetic and potential energy, and the significant height and wave period characterise their value.

Using waves as a renewable energy source has several advantages over other techniques, just as:

- As mentioned before, waves are a result of wind power, which turns out to be formed from solar energy. This way, the usual solar energy intensity of $0.1 - 0.3kW/m^2$ in a horizontal surface is converted into a power perpendicular to the wave propagation, rounding $2 - 3kW/m^2$ [15].
- The available wave energy each season is proportional to the worldwide energy demands [16].
- Unlike solar and wind energy, which has an average availability rounding 20-30 per cent, wave energy is accessible up to 90 per cent of the time [12, 17].
- Waves have a distinct trait where they can travel large distances with little energy lost.

The device that captures this type of energy is called WEC (wave energy converter), and there are numerous different concepts of it. However, they are currently underdeveloped compared to more traditional renewable energy.

2.1.2.1 Potential

An early study made by Isaacs and Seymour [18] predicted that the worldwide potential of wave energy would round between 1-10 TW. To confirm this result, a global study was made using only areas that would supply enough energy to be reliable ($P \leq 5kW/m$) [19].

Even though this result is quite promising, the actual cost to implement such solutions is still not competitive with fossil fuels. However, with recent advances, the cost of implementing this type of device is rapidly dropping to the point that allows this type of technology to enter the market.

2.2 Wave Energy Converter

As mentioned in the subsection 2.1.2, even though this type of energy is quite promising, there are still challenges to overcome to increase WEC performance and commercial competitiveness concerning other types of energy.

The big challenge is converting the random oscillatory force that originates from waves into a motion that can be taken advantage of by a generator. The randomness of the waves derives from their varying height and period throughout the day. To compensate for this issue, using an energy storage unit or another means of compensation is mandatory to convert this varying input into a stable generator input [17].

To improve the captured energy efficiency, prediction models are used to forecast the most common wave power level, in other words, the most common height and wave period. With this wave power level, different WEC designs are suggested.

Another significant challenge to take note of is the fact that even though, for example, on the western coast of Europe, a typical power level rounds 30-70kW/m [17], an unusually high power level of around 2000kW/m could occur in extreme wave conditions. This way, the design has an additional constraint, withstanding this sea state. This challenge brings an economic and efficiency problem since the technology will become more expensive as more resources are used to withstand extreme waves instead of optimising the usual power level.

Considering these constraints, a wide variety of WEC systems were developed over the years, some available on the market and others at a prototype stage. As mentioned before, we can define these concepts using two classifications(location and type) and further specify them with a third classification (mode of operation).

2.2.1 Location

- **Onshore device:** located at the shore and is placed on the bottom of the sea or fixed in a rocky structure. It has the advantage of being easy to maintain and close to the utility network. The downside of this location is that shallow water leads to a lower power supply than in other locations. This kind of device cannot be designed for mass manufacturing because of some fixed prerequisites like shoreline geometry and geology [17].

- **Near-shore device:** located in water depths rounding 10-25m [20], and it is often attached to the seabed to be able to capture most of the energy contained in the waves and just like onshore devices, the shallow water leads to a limited harvesting potential.

- **Offshore device:** located in water depths bigger than 40m [20], and it is either floating or moored to the seafloor. The advantage of being placed in deep water is that it can capture a higher amount of energy. However, this device is more difficult to build and maintain because it has to survive harsh conditions like bigger and more energetic waves [21]. To avoid high maintenance costs, the structure needs to be highly reliable.

The different types of locations and their corresponding wave power can be summarised in Figure 2.2.

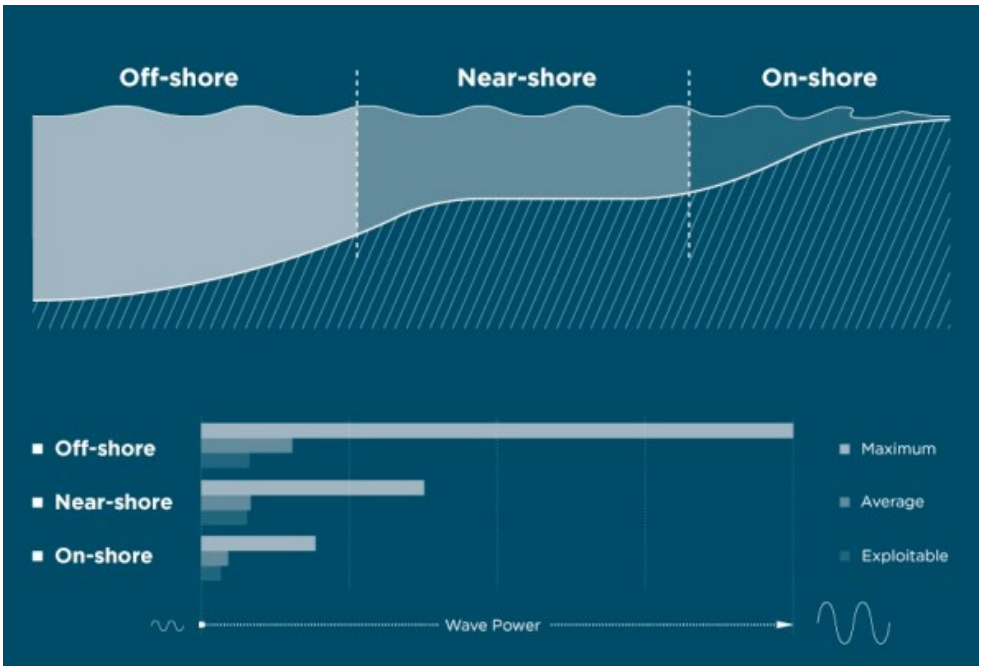

Figure 2.1: Different Locations for WEC with its power levels [1]

2.2.1.1 Type

- **Attenuater:** is a long floating WEC that lies parallel to the primary wave direction and rides it, thanks to its flexibility. The movement generated by the passing waves is strategically restricted to generate energy [22].

- **Point absorber:** is a device whose dimension is much smaller than the wavelength of the waves, it either floats or is attached to the seafloor relying on pressure differential. It typically generates a heave motion that is transformed into linear or rotational motion by mechanical or hydraulic systems to drive electrical generators [21]. The highest performing state is when the wave frequency is equal to the natural frequency of the device, achieving resonance [23].

- **Terminator:** its structure extends perpendicular to the direction of the wave, and as the wave approaches, it is restrained and terminated, capturing its energy [21].

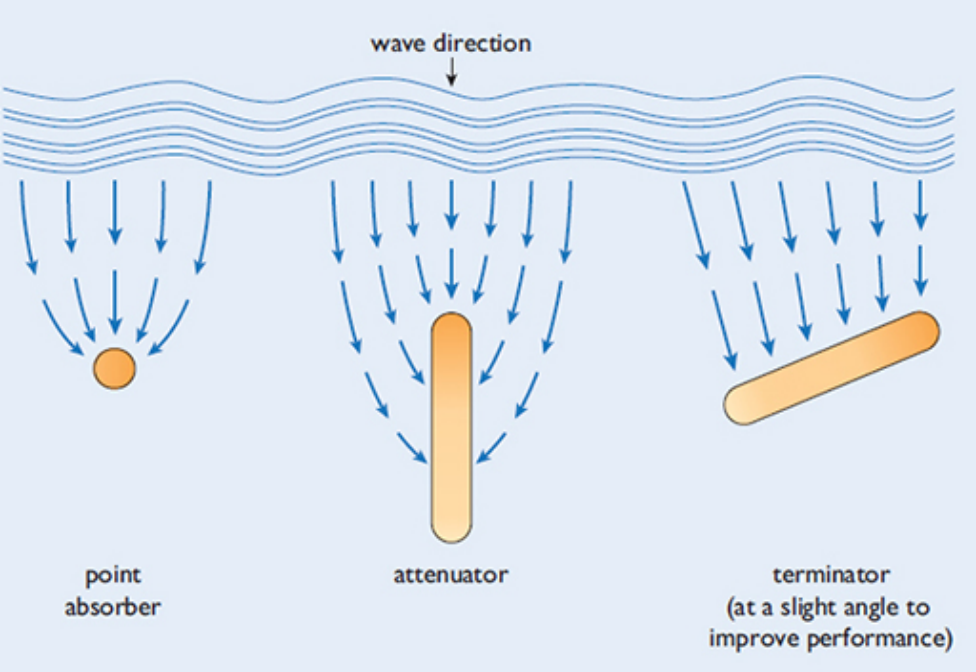

Figure 2.2: Different WEC types [2]

2.2.1.2 Modes of operation

- **Oscillating bodies:** its structure is composed of many units that may move and oscillate around a reference point. The energy in this type of device comes from the body's relative motion produced by the incoming waves concerning its reference point.

- **Oscillating water column (OWC):** mainly consists of a chamber filled with air and seawater and an under the waterline opening that allows waves to change the water level inside its chamber. This water level variation causes the air inside the chamber to compress and decompress as the seawater enters and leaves the chamber. The compressed air exits via a valve above the water column, powering a turbine. The same situation happens with the decompressing air, which causes the air to enter the chamber again through the turbine, originating a bidirectional airflow that generates energy [21].

- **Overtopping device:** consists of long structures designed to physically capture water from waves in a reservoir above sea level. Stored water is returned to the sea from the reservoir via low-head turbines, which generate energy. Its performance can be enhanced using collectors to concentrate incoming waves, leading to higher waves and amplifying the energy captured [21].

These devices operating principle are illustrated in the Figure 2.3

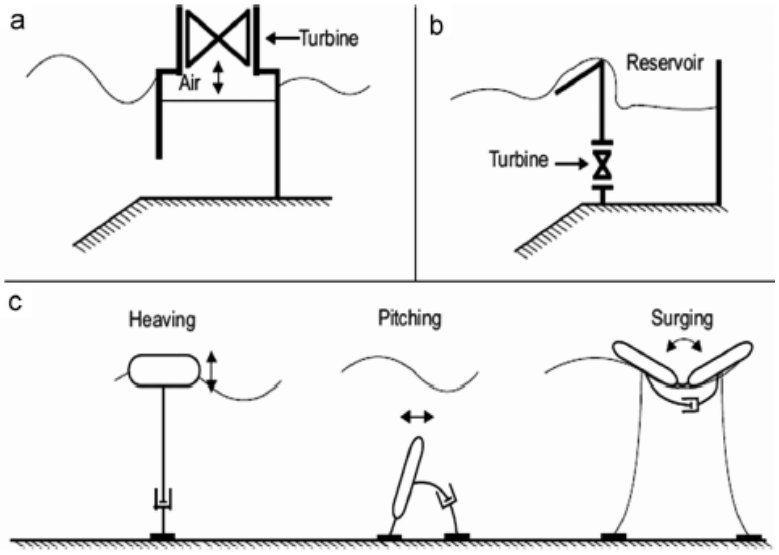

Figure 2.3: Classification of WEC extraction technology: (a) Oscillating water column, (b) Overtopping devices, (c) Oscillating bodies [3]

Chapter 3

State of Art

In this chapter, a review of different OWC technologies and designs is made. Its main objective is to revise and divide the OWC into three parts: its mechanical interface that has been described in the Subsection 2.2.1.2, the power take-off system (PTO), and the control to maximise its energy extraction.

3.1 OWC System Overview

The OWC is a favourite and more promising technology among different WECs. Its attraction comes from the simplicity of the system concept, the ease of integrating into different locations like near and shoreline, and from a mechanical and electrical view, the PTO is reliable since the only moving part (turbine rotor) is working above sea level [5, 11].

This technology can be divided into two main parts: the air chamber and its power take-off system (turbine coupled with a generator). With these two distinct parts, many different designs were proposed by various authors. An initial design consisted of a simple vertical uniform column. However, soon authors realised that with different air chamber designs, the internal sloshing and turbulence could be reduced, leading to higher energy capture ratios [5, 10]. Changing the chamber size and shape to match the device's natural frequency with the frequency of the waves can also lead to a higher energy capture because of a resonance effect.

Another main point of an OWC design is the PTO system. The damping induced by the turbine contributes more to the capture efficiency than the chamber design [24]. This damping influences the water oscillation inside the chamber, therefore the airflow that drives the turbine. Considering this, selecting the correct type of turbine for each OWC is a crucial part of the design.

3.1.1 OWC Architectures

Following the literature, OWC architectures tend to change depending on their location (near or offshore) and the most common sea state.

- **Shoreline Power Plants:** consists of an OWC device integrated into the seacoast, with its bottom side opened into the sea direction to create an air chamber. Some examples are described below:

  - *Pico OWC:* has a $12m \times 12m$ structure ($8m$ water depth) located on the island of Pico in the Azores, where the front wall has a 28° inclination [25, 26]. It is also equipped with a $400kW$ rated Wells turbine-generator set. Studies estimate an annual energy production is rounding $124kW$ when using a specific combination of the turbine rated power and damping coefficient (deduced by simulations). In a Wells turbine, when the flow rate exceeds the stall-free limit, the captured power drops significantly, so to prevent this, a relief valve is used to control this flow rate [26]. It should also be noted that this plant has been closed since October 2018.

  - *LIMPET:* is inclined at a 40° angle to the horizontal, and as mentioned in the section 3.1, this column angle reduces the internal sloshing and turbulence. This device uses a wave breaker on the collector to avoid overtopping the OWC with water. A horizontal bench at the top of the column but under the turbine avoids water inside the turbine. Finally, it also has an external front section with a 60° to the horizontal, that dephases the external and internal water level during the outflow of the chamber to guarantee a continual flow, even if the water level is below the entry point. Just like the Pico OWC, it also uses a relief valve and can produce an annual average of $200kW$ [27]. This plant is located in Islay/Scotland and was decommissioned in 2012.

- **Breakwater Power Plants:** it is similar to the shoreline version, but instead of being integrated with the coast, it is integrated with a newly built breakwater or another coastal protection structure. Its main advantage is the significant price reduction since it utilises an already existing structure. Some examples are shown below:

  - *Mutriku Power Plant:* consists of 16 air chambers integrated into a breakwater, where each one has an individual turbine-generator set with a rated capacity of $18.5kW$, which brings a total capacity of $296kW$. Studies predicted that this 16 turbine-generator set would produce a total of $600kWh$ annually [28], but in reality, only roughly 41% ($246,5kWh$) was produced. This unfortunate result came from the bad design of two air chambers, the maintenance work made throughout the year and the poor system performance when working in extreme conditions [29]. This power plant was also based on the LIMPET and is located in Mutriku/Spain.

- **Floating OWC:** unlike the previous architectures, this new type is not located on a shoreline but the shallow nearshore water ($10-25m$).The main advantage is the higher energy capture since the waves are higher (more energetic), but the device needs to endure a more challenging environment. An example is shown below:

  - *Backward bent-duct buoy (BBDB) OWC:* consists of an L-shaped duct, a buoyancy chamber, an air chamber a typical OWC power take-off system (turbine and generator). Compared to a typical OWC, the wave direction is opposite to the chamber opening [30]. Comparing a forward bent-duct buoy (FBDB) with the BBDB version, studies proved that in terms of energy conversion, BBDB is a considerably superior implementation since its power conversion is only slightly inferior when the wave period is between $11 - 13s$, proving to be way more effective in all others cases [31]. It was also proved that a fixed OWC has a better capture rate in longer waves, while a floating BBDB is better when the wave periods round $5 - 10s$ [31].

- **Multichamber OWC:** consists of an array of air chambers that share a single unidirectional air turbine. Therefore additional rectifying air valves with low-pressure and high-pressure air ducts are needed since an OWC needs to work with bidirectional air flow [5]. An example is shown below:

  - *Seabreath:* works as an attenuator since it utilises an elongated structure with an array of air chambers with an open bottom aligned with the waves. Each chamber will work as an OWC, but in this device, the power take-off system consists of a unidirectional impulse turbine with a high and low-pressure duct. This prototype is still in an early stage since design optimisation is still being done. However, as for today, in an energetic sea, just as in Portugal, estimations predict an annual energy production rounding $850kWh$ [32].

3.2 Power Take-off Overview

Initially, typical unidirectional air turbines equipped with air flow rectifying systems were used on OWC systems. However, it was proven that this type of turbine was unpractical in larger prototypes since the higher flow rate needs an even faster response time that the rectifying systems could not provide.

To solve this problem, self-rectifying air turbines were proposed and tested, divided into two main types: wells and impulse turbines.

3.2.1 Wells Turbine

Wells turbines are based on a lift force applied on rotor blades that are shaped as symmetrical aerofoils, just like in Figure 3.1. The lift force applied on the blades must be higher than the drag force to ensure good efficiency.

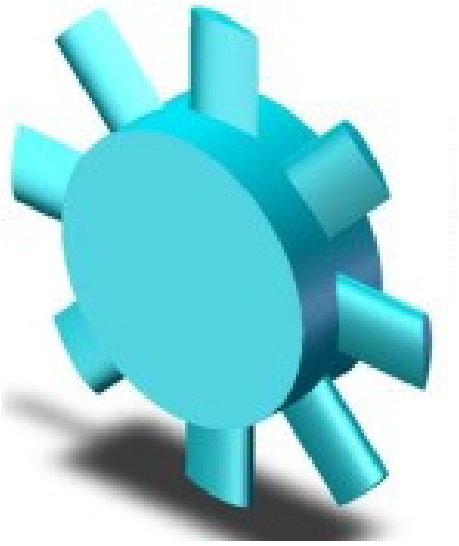

Figure 3.1: Example of a typical Wells Turbine [4]

A Wells turbine efficiency peak rounds 75%, but this effiency tends to drop sharply when the critical angle of airflow incidence is passed. This happens because an aerodynamic stalling occurs when a critical incidence angle is passed. In other words, the lift force decreases sharply, causing a low power efficiency. Therefore there is a fixed interval of airflow values that this type of turbine is suppose to work with.

Different types of Wells turbines were developed just as: with or without guided vanes, bi-plane, contra-rotating and multi stage [33]. The choice of which variant to use depends on the size of the OWC and where it will operate.

Multi-stage Wells turbines can be used if the OWC is placed in a very energetic location, where the device will suffer from excessive centrifugal stress or shock waves. Another application would be in a spar-buoy OWC where the pressure head values are higher than the typical OWC. The only disadvantage of this solution is the higher complexity and costs than a standard wells turbine, so in most cases, an impulse turbine is used instead [4].

The use of guided vanes on both sides of the Wells rotor, as seen in Figure 3.2, has proven to improve the overall efficiency, mainly because there is a lower kinetic energy loss associated with swirling effects [5]. The only disadvantage is an earlier incidence of rotor blade stalling, according to experimental data made by R. Starzmann [34]. Another alternative to produce a similar effect could be using a biplane rotor or a contra-rotating without guided vanes.

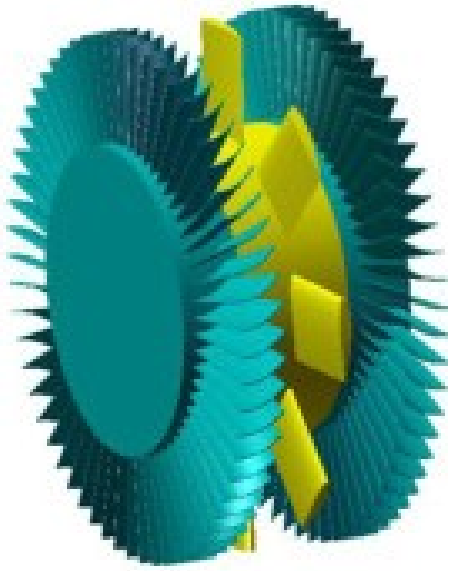

Figure 3.2: Example of a Wells turbine with guided vanes [4]

3.2.2 Impulse Turbine

Impulse turbines can be divided into two main types based on the direction the airflow that passes through it:

- Axial-flow impulse turbine
- Biradial impulse turbine

Guiding vanes can be used on either side of the rotor and can be either fixed, self-pitch-controller or even have a link mechanism.

Axial-flow turbine is usually used because it allows a unidirectional and bidirectional airflow. However, this flow can produce an axial thrust which will cause a fatigue load on the bearings. On the other hand, the radial turbine does not suffer from this fatigue load since it lacks axial thrust. It also has a low manufacturing cost and can achieve a higher torque value. The downside is the high damping induced in the OWC [35].

3.2.2.1 Axial-flow impulse turbine

Self-rectifying axial-flow impulse turbines are the most common alternative to the famous Wells turbine. This device was based on a conventional single-stage steam turbine, but instead of a single row of guided vanes, it uses two to achieve flow direction sensitivity [4]. An example can be seen in Figure 3.3.

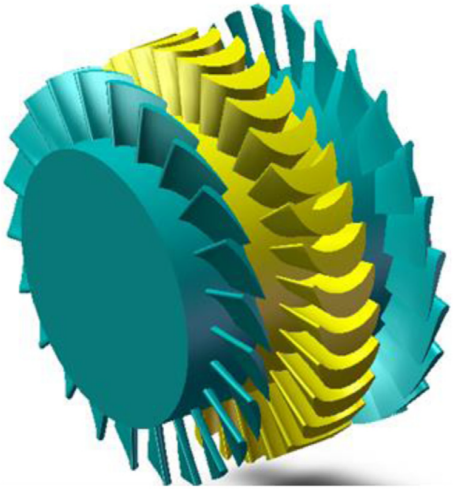

Figure 3.3: Example of an Axial-flow impulse turbine [4]

This type of turbine was developed to overcome some intrinsic disadvantages of the wells turbine: bad starting characteristics, a small range of flow rates where it is usefully efficient and since the rotor blades spin at high speed, there is a consequent noise. At first, the impulse turbine was coupled with a fixed guided vane at a certain angle, but its low peak efficiency caused the development of an impulse turbine with self-pitch controlled guide vanes and subsequently with linked guide vanes [36]. The main disadvantage of this new impulse turbine variant is the maintenance and life cycle problems that add an additional cost to its use [37].

It should also be noted that under irregular waves conditions, following model testing and numerical simulation, the impulse turbine with self-pitch-controlled linked guide vanes has a superior performance relatively to Wells turbine [36]. This result can be justified by the Figure 3.4, which proves that even though the peak efficiency in an impulse turbine is not as high as the Wells, its efficiency stays approximately constant for most air flows values, resulting in higher overall performance. It should also be noted that the simulation made in [36] was in an uncontrolled WEC.

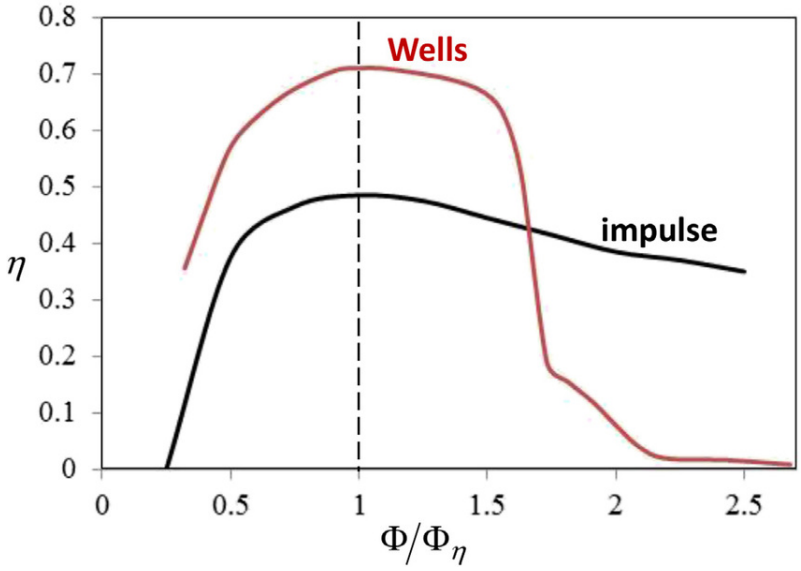

Figure 3.4: Efficiency versus flow rate for Wells and Impulse Turbines [5]

This Figure shows the efficiency, η, versus flow coefficient ratio, $\frac{\Phi}{\Phi_\eta}$ (where Φ_η is the flow coefficient at peak efficiency conditions).

3.2.2.2 Biradial turbine

The Biradial turbine is attractive thanks to its high efficiency and capability, and flexibility to incorporate a high-speed safety valve (HSSV) in its turbine/generator set. This valve enables latching control, one of the most attractive types of WEC Control. It can also leave this valve partially open, resulting in a peak shaving control which limits the available power to be extracted[38].

Its structure is symmetrical with respect to a plane perpendicular to the axis of rotation. It can be divided into two main types: with axially-sliding guide vanes or with fixed guide vanes, where the axially-sliding guide vanes have a higher peak efficiency, around 78% [39], and does not suffer from stagnation pressure loss as the fixed guided vanes. This axially-sliding guide-vanes impulse turbine is shown in Figure 3.5.

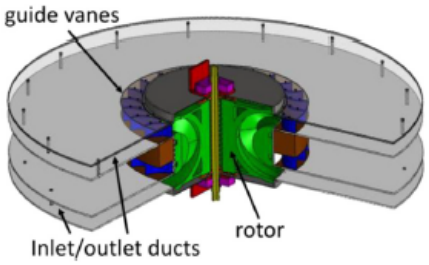

Figure 3.5: Biradial turbine with axially moving guide vanes [4]

The cost of implementing this type of turbine is higher than a typical Wells turbine. However, as shown in Figure 3.6, its peak efficiency is higher, which did not happen in a typical impulse

turbine. With this result in mind and its efficiency remains nearly constant thought the different airflow in the turbine, this developed turbine is superior to the wells in all cases. It should also be noted that the high cost comes from using axially-sliding guide vanes, but for a high-energy environment, its investment is justified [4].

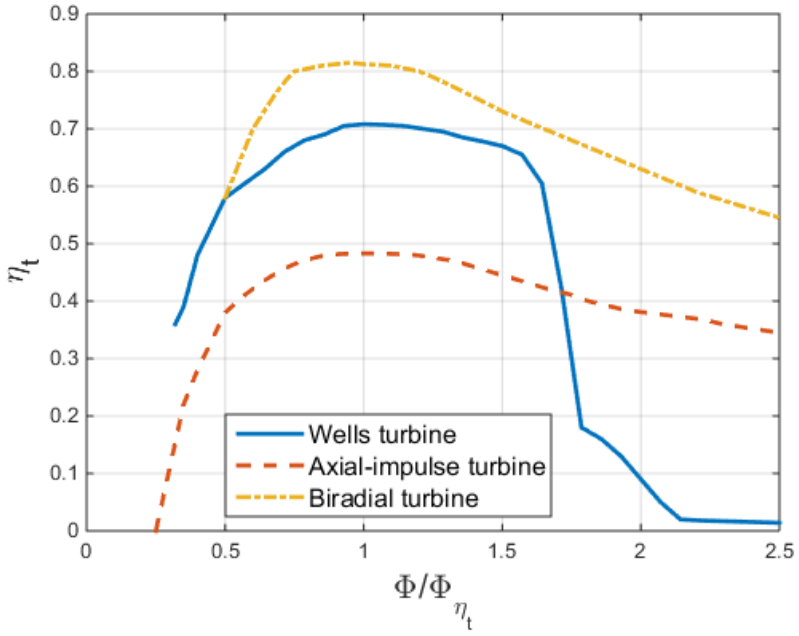

Figure 3.6: The efficiency of Wells turbines, axial-impulse turbines and biradial turbines ploted against the flow coefficient ratio $\frac{\Phi}{\Phi_\eta}$ (where Φ_η is the flow coefficient at peak efficiency conditions) [6]

3.3 Wave Energy Control

Different authors have proposed many different approaches, and a review of those methods' principles is made in [40]. Fundamentally there are two main types of control principles used in an OWC system: stalling prevention control (can be achieved by limiting airflow rate or limiting turbine rotational speed) or latching control (uses a clamping mechanism to bring the WEC into a resonance state with the waves at that present time). Following the review made in [41], this control can be further divided into two categories: predictive control, where the power absorption is maximised over a fixed future time interval, and an adaptive control that adjusts the parameters of a linear WEC model based on WEC responses. This type of control can be achieved using traditional control algorithms, like PID and Fuzzy Logic, and even enhancing these controls with machine learning.

3.3.1 Stalling prevention control

As mentioned before, there are two distinct control methods to prevent staling.

Starting with a turbine rotational speed control, a straightforward approach was made in [42], which uses a Programmable logic controller (PLC) to implement a control law that relates the generator's instantaneous electromagnetic torque with the turbine rotational speed. The equation that relates to the previous variables is the following:

$$T_{ctrl} = a\Omega^b \tag{3.1}$$

where T_{ctrl} denotes the controlled generator electromagnetic torque and Ω is the turbine rotational speed. The parameters a and b are acquired in an offline optimisation. Firstly, a numerical computation is made for each sea state to find the optimal rotational speed that brings the highest averaged power. Then with these various points (Ω, average power), an optimal curve for the equation is traced. Finally, there is also an established limit to the controlled torque to avoid overloading the generator. This approach can also be enhanced using a relief valve, which results in a total increase in annual energy production of about 37%.

A second approach [43] to control the turbine rotational speed utilises a maximum power point tracking (MPPT) strategy to find the optimal rotational speed for each sea state since the sea state influences the mechanical torque. This approach also needs a doubly-fed induction generator (DFIG), which allows rotational speed control by changing the generator slip, coupled with a variable frequency converter in the rotor. This frequency converter has two main elements, the Rotor side converter (RSC) to manage the active (P_s) and reactive power (Q_s) and the Grid side converter (GSC). The RSC establishes an appropriate slip to maintain or force an optimum rotor speed. This author suggests the use of a PI controller in the RSC, which uses the difference between the rotor speed at that time step with the reference rotor speed that brings the optimal rotor speed to compute an appropriate slip to maintain or force an optimum rotor speed.

Similarly, the GSC coupled with a PI controller maintains a direct-current voltage at an established value. This strategy brings a 20.95% efficiency improvement compared to an uncontrolled WEC. However, an air-valve control will be needed in a higher energy sea-state.

Another interesting approach was made in [44], which uses a Fuzzy logic controller (FLC) with precise control rules adjusted to the device site. In this FLC, the input corresponds to the peak value of airflow velocity obtained in the turbine duct of the OWC and the computed output will be an external rotor resistance value. This variable external resistance value changes the rotor slip. In other words, it changes the rotor rotational speed. Simulations with regular waves show a 40.5% improvement in the generated power compared to an uncontrolled plant since staling is wholly avoided. Irregular waves were also tested, achieving slightly worst results, but they were still very promising. This control can also be achieved by a neural network [45], which will bring better results, but the time consumed to train this neural network in different environments is way higher than to change some fuzzy set rules depending on the location of the OWC site.

As mentioned, stalling control can also be done by limiting the airflow in the OWC. That is what the method in [46] does, where it takes advantage of an adaptive PI controller, which creates an opposing force to the OWC oscillations, also known as a damping force. A traditional PI

controller could also be used [47], but as the sea conditions change over time, the P and I gains should be adjusted for higher efficiencies, which is where the adaptive PI shines. The main idea is to optimise the gains using a look-up table for each time step, where the critical variable is the real-time estimate of the dominant wave frequency of the wave force. The author of this approach compared this adaptive PI with a classic PI and a switching gain-scheduled PI, and the adaptive PI outperformed both methods in an irregular wave environment. A similar approach was made by S.K. Mishra [48], which uses a Fractional order PID (FOPID) to control air valves to limit excessive airflow through the turbine, preventing the stalling phenomenon. A FOPID was chosen instead of a classic PID since it improves the control law, less disturbance and a better output regulation [49]. As the valve area varies with the control output, there will be a limit to this value since the valve cannot close or open more than its limit. The problem with this output saturation is that the error can reach a value that the control action cannot cover. Therefore, the error will reach a limit, and the integral value will keep rising, leading to an unstable control. This can be overcome by using an anti-windup FOPID, which will reset the integral value and prevent the controller output from wandering away.

Another proposal was made by A. F. de O. Falcão [50], which uses a by-pass air valve coupled with a wells turbine. As seen in Figure 3.4, the turbine efficiency drops sharply as the flow rate increases, so the valve is used to avoid this limitation, in other words, to avoid over-pressuring the OWC air chamber since it is directly proportional. This air valve is controlled using a limit for the pressure inside the air chamber, in other words, a limit to the turbine pressure head, with will open if this limit is surpassed therefore maintaining the pressure at a high-efficiency point. It also uses an M number of valves of the same size, which allows controlling how much area is used to control the total flow rate that exits through the valves. A PLC predicts when the pressure exceeds the imposed limit and how much total area should be opened to maintain the pressure at that high-efficiency limit. After reaching this limit, at each time step, the PLC also computes how much opened area is needed until a completed closure, resetting the process. This way, the estimated annual energy production was increased by 25%. However, this result is not trustworthy since the valve flow rate was assumed to vary at a linear pace during its control when real valve behaviour differs depending on its geometry and actuation principle.

3.3.2 Latching control

Budal and Falnes were the first to introduce the latching control in 1980 [51], using a simple buoy system, where the energy extraction was optimised by locking and realising the buoy movement so that the buoy movement was in phase with the wave excitation force, achieving resonance. In 2006, Babarit and Clement [52] adapted this control for an oscillating-body WEC. Finally, in 2016, Henriques *et al.* [53] also used this latching control but focused on an OWC system.

This type of control has been designated as a non-causal control. That is, the input values of the control algorithm come from future predictions instead of present or past values. In this case, wave force predictions are made and can be classified into two different groups. The first is spatial

prediction, where the forecast is made using wave information from close locations. The second one predicts the wave excitation force using recent past values of the waves at that exact location.

A recent exciting approach for this type of control was made in [54], where a real-time latching control was implemented since the optimal control proposed by Babarit and Clement [52] was unreliable in a natural environment because knowing a priori the entire wave force during the WEC operation is impossible. Therefore, the real-time latching control maximises the power absorption by executing the control action in real-time, gradually moving the time horizon forward instead of having the control action predefined for the chosen time interval. Since predicting the wave force for the entire working duration is unreliable, a wave prediction model for a shorter time interval based on grey model [55] was used. This model uses past consecutive data from WEC motion and the wave force to predict future values in a short horizon. It should also be noted that using too many past data points or increasing the prediction time interval will lead to less accuracy. Simulation results demonstrated that this approach produces up to 40% more power than an uncontrolled WEC. Another interesting point taken from the results is that a longer receding horizon length is more beneficial than a concise one since, in the shorter one, hardly any control action is made (the floater is released most of the time). However, as the prediction increases the receding horizon length, more accumulated errors occur, so there will always be a trade-off between forecasting length and forecasting precision. This approach author, Liang Li, also tested another way to predict wave forces using an artificial neuronal network, achieving a better prediction ability [56].

There was also a study made by F. Saupe *et al.* [57], which compares a predictive latching control just as mentioned before [52] with a PTO velocity PI controller. The simulation results with irregular waves show that the predictive control outperforms the PI control when considering the energy loss from transforming mechanical energy to electrical.

A similar control method is declutching. Instead of decreasing the peak PTO moment as the latching control, it will increase this peak. The declutching consists of connecting and disconnecting the control system during part of the wave cycle to control the phase response of the WEC. This will lead to a higher magnitude motion inside the WEC and phase matching with the wave cycle, resulting in higher absorbed energy. Another vantage is that there will not be any negative or reactive power flow, but the control action will consume energy. An amusing proposal was made by Enrico Anderlini [58], who used Reinforcement learning to implement this declutching control, where a defined number of wave cycles defines each training episode. Throughout each episode, the possible states are defined by the WEC motion position, its velocity and the current sea state, and the possible action is to turn on or off the control. The study concluded that although the increased power absorption was not so high as in latching control, it is way easier to implement since it does not depend on the model device dynamics.

Chapter 4

Modelling

In this chapter, an OWC model is exposed, with its following equations and the relations between each sub-system, to give a solid understanding of how the system works and is modelled.

4.1 OWC Model

The OWC wave-to-wire model was taken from [59], which uses a Mutriku OWC power plant as a test case to explain the OWC performance based on each sub-system's physical behaviour.

The OWC system can be divided into three different sub-systems:

- Air chamber pressure model
- OWC hydrodynamic model
- Power take-off model

The following chapter will highlight each sub-system to explain its principles further.

4.1.1 Air chamber pressure model

The instantaneous air chamber volume is computed as:

$$V_c = V_0 - zS \tag{4.1}$$

where the V_0 is the air volume inside the chamber in calm water, S is the cross-sectional chamber area, and z is the instantaneous position of the imaginary cross-section between the air and the water level in the chamber.

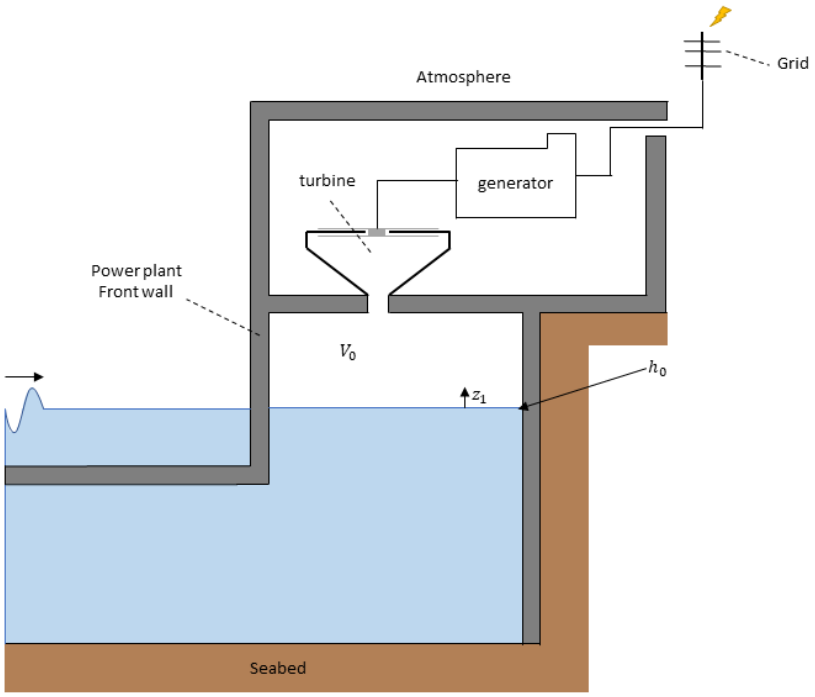

Figure 4.1: OWC Schematic

The instantaneous mass inside the air chamber is computed as $m_c = \rho_c V_c$, where the air density inside the air chamber is determined as:

$$\rho_c = \rho_{at}(p^* + 1)^{1/\gamma} \tag{4.2}$$

where $p^* = p/p_{at} - 1$ is the dimensionless relative pressure oscillation inside the chamber and γ is the specific heat ratio, p_{at} is the absolute atmospheric pressure and p_{at} is the air density in atmospheric conditions.

The air pressure inside the air chamber, assuming an isentropic compression/expansion, is related to the mass flow rate of air through the air turbine ($\dot{m_{turb}}$), just as:

$$\frac{\dot{p}^*}{p^* + 1} = \gamma\left(\frac{\dot{V_c}}{V_c} + \frac{\dot{m_{turb}}}{m_c}\right) \tag{4.3}$$

4.1.2 OWC hydrodynamic modelling

The OWC motion equation is computed as:

$$(m + A^\infty)\dot{v} = -\rho_w g S - p_{at} S p^* + F_d - R \tag{4.4a}$$

$$\dot{z} = v \tag{4.4b}$$

where m is the mass of the water displaced by OWC chamber, A^{∞} is the added mass at infinite frequency (obtained from an AQWA simulation), ρ_w is the water density, g is the gravity acceleration. It should also be noted that v is the instantaneous velocity of the imaginary cross section between the air the the water level in the chamber.

The excitation force, F_d, induced on the imaginary piston between the air and sea level inside the chamber, can be computed as a sum of N components of a ω_n frequency (different wave frequencies):

$$F_d = \sum_{n=1}^{N} A(\omega_n)\Gamma(\omega_n)cos(\omega_n t + \phi(\omega_n) + \phi_r(\omega_n)) \tag{4.5}$$

where $A(\omega_n)$ is the wave amplitude as a function of the wave frequency obtained from a JONSWAP spectra, $\Gamma(\omega_n)$ is the piston heave excitation force, ϕ_r the excitation response to the wave component and ϕ is a random phase generated.

The radiation force, R, is defined as:

$$R = \int_0^t \chi(t-s)vds \tag{4.6}$$

where $\chi(t)$ is the impulse function of the piston motion. This convolution integral 4.6 can be computed as a linear state space form, obtained from the added mass and radiation damping coefficients.

The hydro-static force can be computed by $\rho_w gS$, and the force applied by the pressure inside the chamber is calculated as $p_{at}Sp^*$.

4.1.3 Power take-off model

4.1.3.1 Turbine/generator set modelling

The turbine/generator set's dynamics were modelled using the relationship:

$$\frac{d}{dt}\left(\frac{1}{2}I\Omega^2\right) = P_{turb} - P_{ctrl} \tag{4.7}$$

where P_{turb}, P_{ctrl},I and Ω is the instantaneous turbine aerodynamic power, the instantaneous generator electromagnetic power imposed to control the rotational speed, the inertia and the turbine rotational speed, respectively.

4.1.3.2 Turbine modelling

The turbine behaviour is modelled using two performance characteristics of an air turbine, as functions of the dimensionless pressure head, Ψ:

$$\phi = f_\phi(\Psi) \tag{4.8a}$$

$$\pi = f_\pi(\Psi) \tag{4.8b}$$

where:

$$\Psi = \frac{\Delta p}{\rho_{in}\Omega^2 D^2} \tag{4.9a}$$

$$\phi = \frac{\dot{m_{turb}}}{\rho_{in}\Omega D^3} \tag{4.9b}$$

$$\pi = \frac{P_{turb}}{\rho_{in}\Omega^3 D^5} \tag{4.9c}$$

The ϕ is the dimensionless flow rate, π is the power coefficient, $\Delta p = p_{at}p*$ is the stagnation pressure head between the air chamber and the atmosphere, ρ_{in} is the turbine inlet density at stagnation conditions, and D is the rotor diameter.

The performance characteristics values are calculated using interpolation on the following image curves:

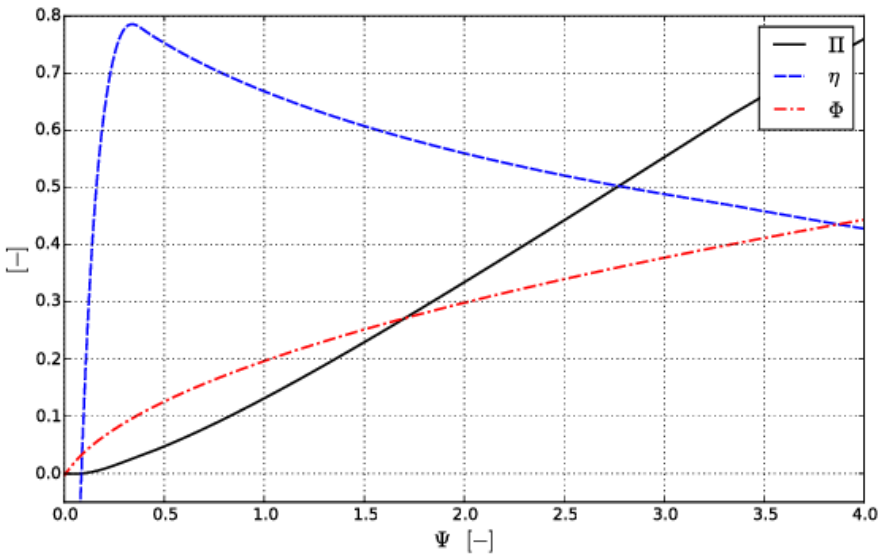

Figure 4.2: Dimensionless flow rate, ϕ, dimensionless power coefficient, π, and efficiency, η, as functions of the dimensionless pressure head, Ψ, for the biradial turbine used in the numerical simulations [7]

At last the reference density, ρ_{in}, depends if the turbine is at an exhalation oh inhalation phase:

$$\rho_{in} = \begin{cases} \rho_c & if\, p^* > 0 (exhalation) \\ \rho_{at} & if\, p^* < 0 (inhalation) \end{cases} \tag{4.10}$$

From the equation 4.9c, the turbine aerodynamic power can be computed as:

$$P_{turb} = \rho_{in}\Omega^3 D^5 f_\pi(u\Psi) \tag{4.11}$$

where its assumed that the turbine is equipped with a safety valve, where $u = 1$ corresponds to an opened valve and $u = 0$ to a closed one leading to a safe mode operation.

4.2 Electrical generator modelling and control

One of the most simple and effective control law can be derived from simple physical arguments. Based on the equation 4.7, assuming that the inertia is null, the instantaneous turbine aerodynamic power equals the instantaneous generator electromagnetic power. Then if we maximise the turbine efficiency from the best efficiency point Ψ_{bep}, the turbine power can be the following:

$$P_{turb}(\Psi_{bep}, \Omega) = \underbrace{\rho_{in} D^5 f_\pi(\Psi_{bep})}_{a_{bep} \approx \text{constant}} \Omega^3 \tag{4.12}$$

where a_{bep} is approximately constant since the turbine inlet density (ρ_{in}) is much smaller in computation to the turbine rotational speed variations. This way, the generator power can follow the following relation:

$$P_{ctr} = a_{bep} \Omega^3 \tag{4.13}$$

In reality, assuming the turbine inertia equal to zero is very unrealistic and considering the relationship between turbine aerodynamics and OWC hydrodynamics, a more generalised control equation can be:

$$P_{ctr} = a \Omega^b \tag{4.14}$$

A simple control law to avoid overloading the generator imposes a limit to the P_{ctr}:

$$P_{ctr} = min(a\Omega^b, P_{gen}^{rated}, T_{gen}^{max} \Omega) \tag{4.15}$$

where P_{gen}^{rated} is the generator rated power and T_{gen}^{max} the maximum allowed torque:

$$T_{gen}^{max} = \frac{P_{gen}^{rated}}{\omega_{gen}^{nom}} \tag{4.16}$$

where ω_{gen}^{nom} is the nominal angular speed where the generator is at its rated power, and since $\omega_{gen}^{nom} = \frac{2\pi\Omega_{gen}^{nom}}{60}$, the T_{gen}^{max} can be computed as:

$$T_{gen}^{max} = \frac{60 P_{gen}^{rated}}{2\pi\Omega_{gen}^{nom}} \tag{4.17}$$

where Ω_{gen}^{nom} the nominal rotational speed where the generator is at its rated power.

Another essential restriction of the generator is that if its rotational speed surpasses a specific limit, Ω_{ctrl}^{max}, the centrifugal stress becomes unbearable. At the same time, to minimise flow compressibility effects on the turbine rotor blades, such as shock waves, the Mach number depending

on the tip speed must also be limited. If a maximum blade speed of about $\Omega D/2 = 160m/s$, then the maximum rotational speed is computed as:

$$\Omega_{ctrl}^{max} = min(\Omega_{gen}^{max}, 320D^{-1}) \tag{4.18}$$

This way if the turbine rotational speed surpasses the defined max, the turbine closes the valve, operating at a safe mode ($u = 0$). The turbine only returns to its normal mode ($u = 1$) when its turbine speed becomes lower than a threshold (Ω_{thr}), derived from the Ω_{bound}, where:

$$\Omega_{thr} = 2^{-1/b}\Omega_{bound} \text{ [59]} \tag{4.19}$$

4.2.1 Control using an ANN with a local maxima algorithm to determine PTO parameters

As seen in the equation 4.14, this control law has two parameters (a,b), which can be sensitive to the actual sea state (Hs: Significant wave height, Te: Wave energy Period). Assuming this, one way to control this PTO system can be by utilising an Artificial Neurol Network (ANN) with a local maxima algorithm to calculate the optimal PTO parameters in the next time horizon. The following Figure 4.3 and Algorithm 1 shows the following control:

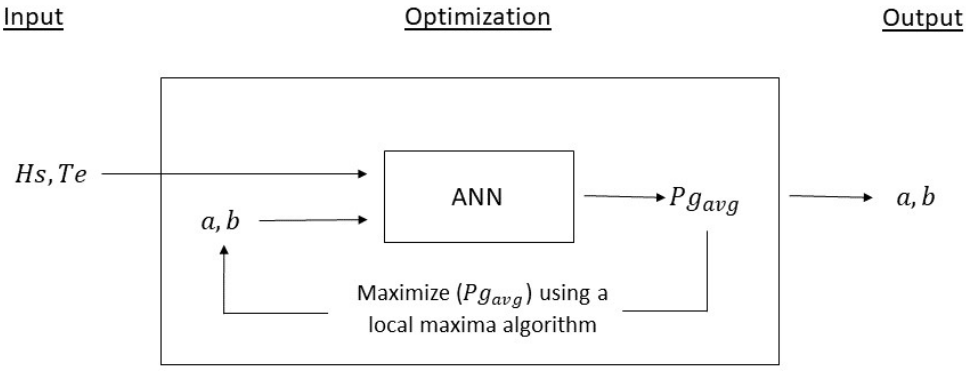

Figure 4.3: PTO optimization using a ANN with a local maxima algorithm

Algorithm 1 Control using an ANN with a local maxima algorithm to determine PTO parameters

1: Identification of the Sea State (Hs,Te)
2: Search for the optimal turbine parameter(a,b),using a local maxima algorithm with the ANN with the inputs(a, b, Hs, Te) and output (Pg_{avg})
3: Application of the optimal turbine parameters calculated
4: Next time step (jumps to 1)

It should also be noted that the average generated power(Pg_{avg}) is defined as:

$$Pg_{avg} = \frac{1}{t_f - t_i}\int_{t_i}^{t_f} Pg(t)dt \tag{4.20}$$

4.2.2 Control PTO system through a PID Controller

Another way to control the extracted energy from the OWC power plant can be done by controlling the turbine's rotational speed through a PID controller.

This approach uses the rotational speed which brings the turbine to its highest efficiency point, Ω_{bep}, is calculated using the equation 4.11:

$$\Omega_{bep} = \sqrt{\frac{\Delta p}{\rho_{in} \Psi_{bep} D^2}} \tag{4.21}$$

and will be used as the error reference for the PID controller.

The difference between the optimal rotational speed and the actual will be used to compute the generated power, P_{ctr} which is also imposed by the Equations 4.14 and 4.15. Following this new imposed P_{ctr}, a new rotational speed is calculated through the Equation 4.7. This type of control is shown in the following Figure 4.4:

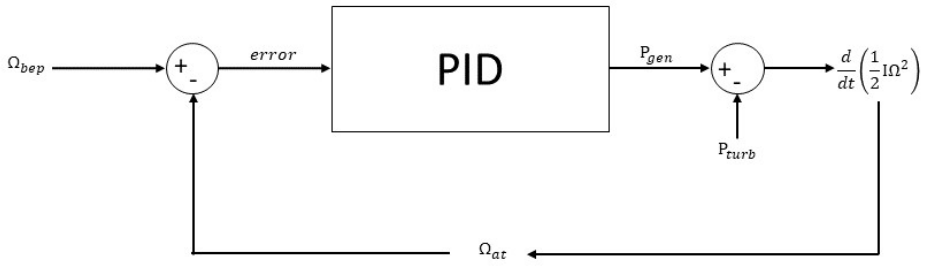

Figure 4.4: PID control for the OWC

It should also be noted that the OWC system and dynamic between the optimal and current turbine speed are not linear, so finding a transfer function to represent it is very difficult since there is no known linear model. Therefore, classical PI tuning is not possible. To overcome this problem, an algorithm to find the best parameters for each sea state must be used, just like a genetic or a particle swarm algorithm (PSO). In this case, a PSO algorithm was used where the optimisation criteria used was the integral of absolute error (IAE):

$$\int_0^t |e(t)|\, dt \tag{4.22}$$

where the $e(t)$ is the error used as an input for the PID.

The used PID model in the Simulink environment has 4 tuning parameters:

- P: Proportional Gain
- I: Integral Gain
- D: Derivative Gain

- N: Filter coefficient

which means that the PSO algorithm will find the 4 best parameters for each sea state

Another important point about using this PID is that the PID output will saturate since there is a limit on how much the generator can produce, imposed by the control rule 4.15. This means that, for example, when the output remains at a saturated positive level, the feedback becomes broken since the integral part increases as the error also remain positive, leading to an unstable control. This can be overcome by using an anti-windup, which resets the integral value and prevent the controller output from drifting. In this case, the anti-windup method chosen was the back-calculation, which uses a tracking time constant, T_t, to determine the rate of resetting the integral term of the controller. This parameter should be larger then the derivative time, $T_d = \frac{D}{P}$ and smaller than the integral time, $T_i = \frac{P}{I}$ [60], therefore it can be computed as:

$$T_t = \sqrt{T_i T_d} \tag{4.23}$$

Chapter 5

Case of Study

In this chapter, a description of the methods and procedures utilised in this work is described. The author pretends to provide the reader with information on the study's methodology.

5.1 Mutriku Wave Power Plant

As mentioned in the previous Chapter 4, the Mutriki Wave Power Plant will be used as a base to study the behaviour of different control methods. Therefore a physical description must be made to validate this study.

5.1.1 Variables

Its geometry consists of a rectangular structure with a width of 4.3 m and a length of 10 m resulting in an area of 43 m^2 relatively to the water plane where the imaginary piston is, and a front wall with 12.885 m height as seen in the Figure 4.1, where is assumed that the initial piston position is when the shallow waters are at 6.45 m. The following OWC model was implemented in a Matlab/Simulink system with the following parameters:

Variable	**Value**
P_{at}	1.01325×10^5 *Pascal*
ρ_w	1.201 kgm^{-3}
ρ_{at}	1025 kgm^{-3}
g	9.81 ms^{-2}
$heat_{ratio}, \gamma$	1.4
m	87217 g
A^{∞}	633190 g
S	43 m

Table 5.1: OWC hydrodynamic and aerodynamic model parameters

It should also be noted that the following turbine/generator set characteristics were withdrawn from the installed one at the site and deduced from the mathematical expressions in the Section 4.2:

Variable	Value
$Diameter, D$	$0.5\ m$
$Inertia, I$	$5.01\ kg\ m^2$
a_{ref}	$1 \times 10^{-}3$
b	3
Ψ_{bep}	0.335
P_{gen}^{rated}	$30\ kWg$
Ω_{gen}^{nom}	$1470\ RPM$
Ω_{bound}	$200\ RPM$
Ω_{th}	$158.74\ RPM$
T_{gen}^{max}	$194.8\ Nm$

Table 5.2: Turbine/Generator parameters

The Figure 4.2 highlights that the highest turbine efficiency point is at $\Psi_{bep} = 0.335$, with an η rounding the 0.7879. The rotational speed threshold from the Equation 4.19, using an $\Omega_{bound} = 200\ RPM$ has a value of $158.74\ RPM$. At last, the T_{gen}^{max} was computed using the Equation 4.17, leading to a value of $194.8\ Nm$.

5.1.2 Sea States

The wave energy was modelled using 14 different sea states available at the Mutriku power plant, which are defined by the significant wave height (H_s), wave energy Period (T_e), and frequency of occurrence (f_o). The following table demonstrates those sea states:

n	H_s [m]	T_e [s]	f_o [%]
1	0.88	5.5	3.23
2	1.03	6.5	3.44
3	1.04	7.5	5.08
4	1.02	8.5	6.11
5	1.08	9.5	10.73
6	1.19	10.5	9.31
7	1.29	11.5	9.52
8	1.48	12.5	7.42
9	1.81	13.5	2.75
10	2.07	14.5	2.96
11	2.59	15.5	1.34
12	2.88	16.5	0.4
13	3.16	11.5	0.27
14	3.2	12.5	0.42

Table 5.3: Sea states of Mutriku Power Plant

This sea states, as described in Section 4.1, with the JONSWAP spectrum will compute the wave energy for each sea state to be used in the excitation force 4.5. It can also be used to calculate

the available wave energy force (F_w) per meter [61]:

$$F_w = \frac{\rho_w g}{64} H_s^2 D_w \tag{5.1}$$

where the D_w is the wavelength, which is computed as: $\frac{gT_e^2}{2\pi}$.

The available wave energy power (P_w) per meter can be computes as: $F_w \times v_w$, where v_w is the wave velocity. If assumed that the wavelength can also be written as $D_w = v_w \times T_e$, then the P_w can be computed as:

$$P_w = \frac{\rho_w g^3}{128\pi^2} H_s^2 T_e \tag{5.2}$$

5.2 Simulink Implementation

As mentioned before, the full model can be divided into three different sections: air chamber pressure, OWC hydrodynamic and power take-off model, as in the Section 4.1. Therefore, the Simulink model will be divided just like that:

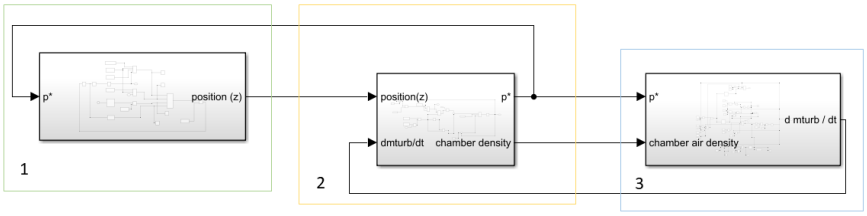

Figure 5.1: Full Simulink Model

As seen in Figure 5.1, the green rectangle (1) corresponds to the OWC hydrodynamic model, the yellow one (2) to the air chamber pressure model and the blue one to the power take-off model (3). It should also be noted that in all the simulations, the chosen ordinary differential equation solver was an ODE3 with a fixed time-step of 0.001 s for a time period of 1500 s.

5.2.1 Air Chamber Pressure Model

Starting with the description of the air chamber pressure model in the Simulink, as seen in the Figure 5.2:

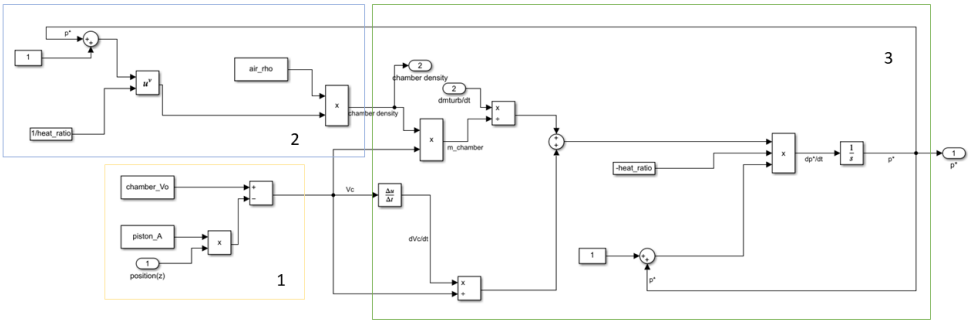

Figure 5.2: Air Chamber Pressure Model

the yellow rectangle (1) corresponds to the Equation 4.1 (chamber volume), the blue rectangle (2) corresponds to the Equation 4.2 (air chamber density) and the green rectangle (3) corresponds to 4.3 (relative pressure).

5.2.2 OWC Hydrodynamic Model

Following with the description of the OWC hydrodynamic model in the Simulink, as seen in the Figure 5.3:

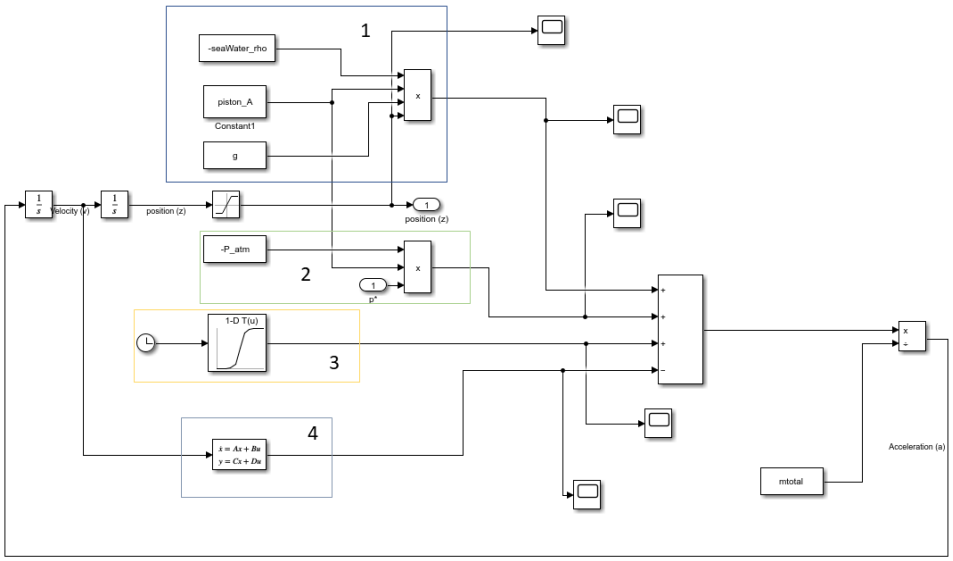

Figure 5.3: OWC Hydrodynamic Model

Considering the Equation 4.4 (hydrodynamic forces) and comparing it to the previous Figure, it can be noted that the blue rectangle (1) corresponds to the hydro-static force, the green rectangle (2) to the force applied by the pressure inside the chamber, the yellow rectangle (3) to the excitation force and the grey rectangle (4) to the radiation force.

The excitation force is computed by interpolating discrete data points, given by the Equation 4.5 throughout each time-step. The radiation force mentioned in 4.1 is represented as a

state-space model, which produces the respective radiation force using the actual imaginary piston velocity as an input.

5.2.3 Power Take-off Model

At last, the PTO modelling in the simulink is confirmed in the Figure 5.4:

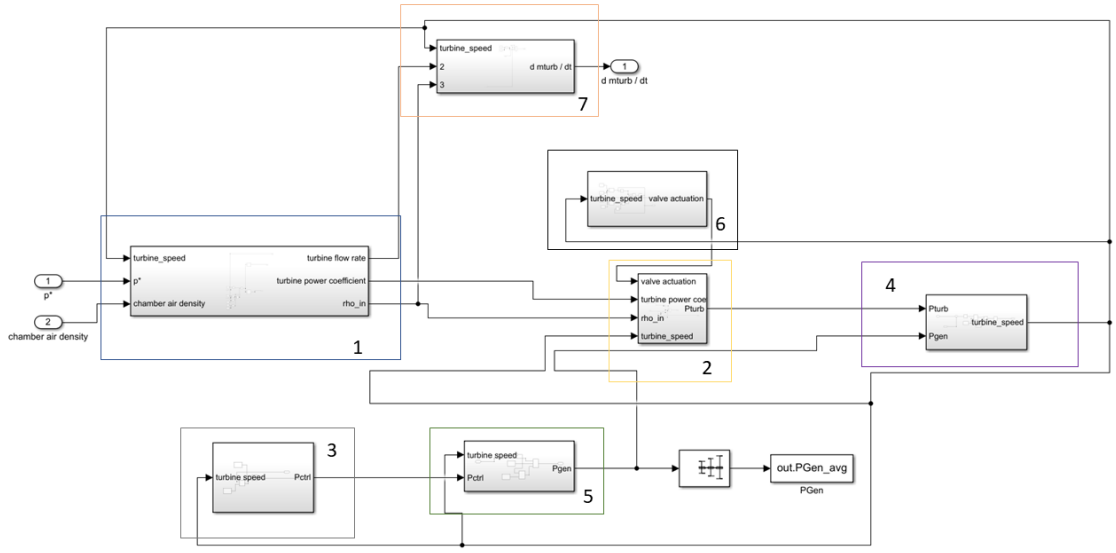

Figure 5.4: Power Take Off Model

the blue rectangle (1) correspond to the performance characteristics of the biradial air turbine 4.2, where the pressure head, Ψ, is computed by the Equation in 4.9, the turbine power coefficient, π, and the flow rate, ϕ, are calculated using an interpolation their respective curves in 4.2. Note that these variables are all dimensionless. The following Figure 5.5 corresponds to the blue rectangle Simulink model:

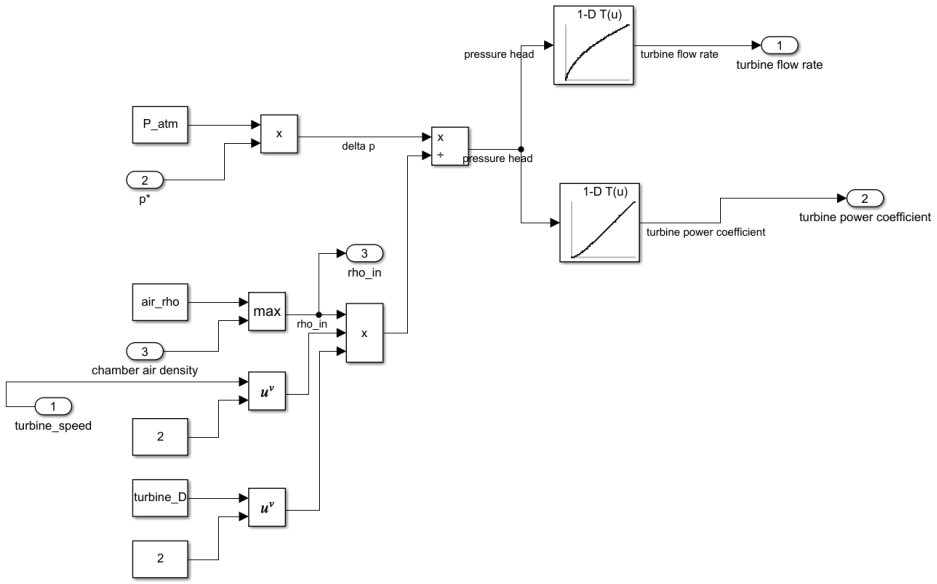

Figure 5.5: Simulink model of the Turbine Performance Characteristics

The yellow rectangle (2) is the computation of the turbine power through Equation 4.11, the grey rectangle (3) is the power generated using the control law, P_{ctrl}, just as in Equation 4.14 and the purple rectangle (4) is the calculation of the turbine rotational speed, Ω, using the relation 4.7. The following Figure 5.6 corresponds to the yellow, grey and purple rectangles Simulink models:

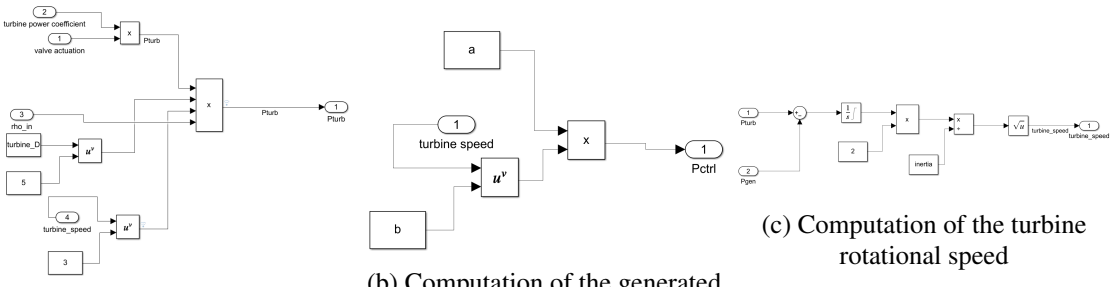

(a) Computation of the turbine power

(b) Computation of the generated power

(c) Computation of the turbine rotational speed

Figure 5.6: Simulink model of the turbine,generated power and rotational speed computation

The green (5) and black (6) rectangles corresponds to the generator overload protection 4.15 and the rotation speed protection 4.17 respectively. The following Figure 5.7 corresponds to the green and black rectangles Simulink models:

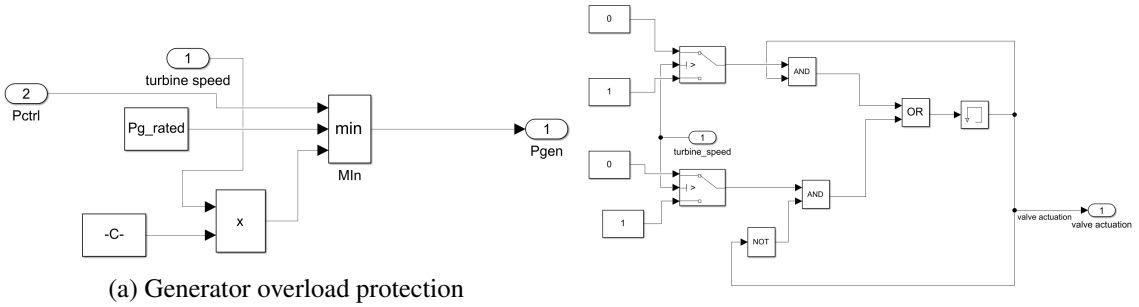

(a) Generator overload protection

(b) Rotation speed protection with valve actuation

Figure 5.7: Simulink model of the generator overload protection and the rotation speed protection with valve actuation

At last, the orange rectangle (7) is used to compute the mass flow rate of air through the air turbine ($\dot{m_{turb}}$), to later be used in the air chamber pressure model block. The following Figure 5.8 corresponds to the orange rectangle Simulink model:

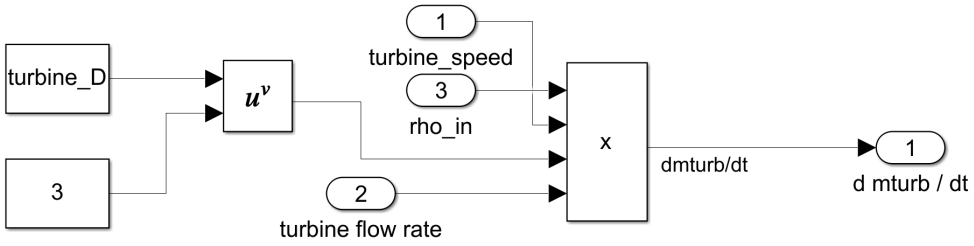

Figure 5.8: Simulink model of the computation the mass flow rate of air through the air turbine

5.3 ANN Optimisation and final architecture

In order to find the most optimal ANN architecture, the most crucial factors are the number of hidden layers, the number of neurons at each layer and the activation function. In this case, as mentioned in 4.2.1, the objective of this ANN is to make a regression to predict each average generated power so that the hidden layers can use a non-linear activation function: rectified linear activation unit (ReLU), as seen in the Figure 5.9, since the sigmoid and hyperbolic tangent functions shouldn't be employed in networks with many layers due to the vanishing gradient problems. Due to this advantage, it allows for faster training and better performance overall. The output activation function will be the linear function.

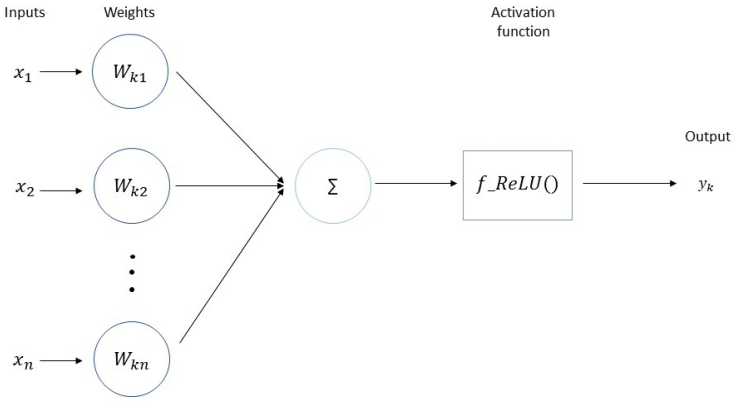

Figure 5.9: Neuron Example, with the Relu activation function

There is also the issue where there is not a perfect number of hidden layers and the number of neurons at each layer. So to overcome this issue, instead of randomly assigning a number for these two parameters and checking if the neural network performance is acceptable, it is more efficient to develop a script to incrementally test a range of different parameters and evaluate each different set. The following python script with TensorFlow, as shown in the code-block A.5, creates all the different architectures to be later tested:

After obtaining all the different models, the training is done using the loss function mean absolute error, the optimiser is the RMSprop, and the metric is a binary accuracy through mean absolute error, as seen in the code-block A.6.

This script returns all the trained models with the mean absolute error computed, which will be used to compare them all and choose the one with the better performance. This resulted in an architecture composed of 4 inputs, 3 hidden layer, where the first two layers have 64 neurons, and the last hidden layer has 192 neurons and 1 output, with a mean absolute error, MAE, of 2.3838×10^{-04}. The resulting model is illustrated in Figure 5.10.

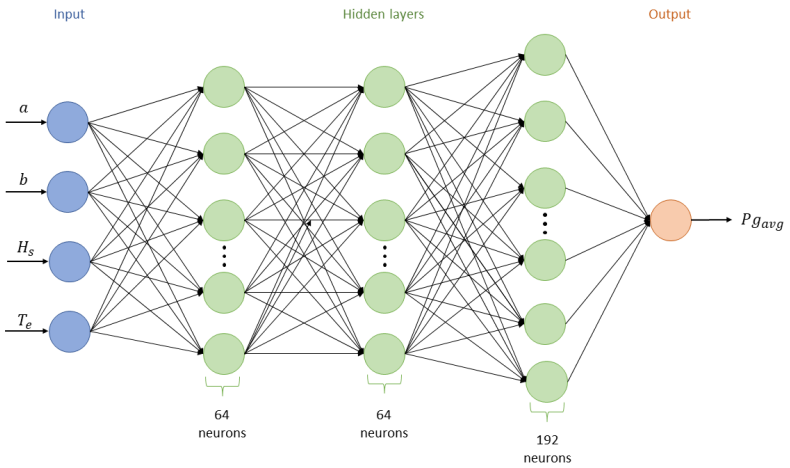

Figure 5.10: Full Architecture Optimised

It should be noted that the Data set collected to train and test this ANN model was obtained by simulating the Simulink model presented in Section 5.2, using the Matlab script A.2. Throughout all 14 sea states described in 5.1.2, the control parameters a and b were varied in $[1 \times 10^{-}4, 2 \times 10^{-}3]$ and in $[2.5, 3.2]$, respectively, since these values are the typical variation in the generator control law parameters. This results in $3731(80\%)$ training points and $931(20\%)$ testing points, where each simulation had a time span of 1500 s and a time-step of 0.001 s. Another important aspect is the normalisation and shuffling of the data set that was done. Normalisation reduced the computation time, and if a data set feature is large in scale compared to the other features, it would become dominating and lead to an inaccurate ANN. Shuffling data reduced its variance, generalised the model and prevented overfitting.

5.4 PID Model

As mentioned in Section 4.2.2, instead of the simple control law 4.14, the imposed generated power is replaced by a PID Controller, which uses the Ω_{bep} as the reference to optimise the turbine efficiency. The new PTO Simulink model is illustrated bellow 5.11, where the blue rectangle (1) corresponds to the computation of the rotational speed, which brings the best turbine efficiency, and the green rectangle (2) corresponds to the PID controller:

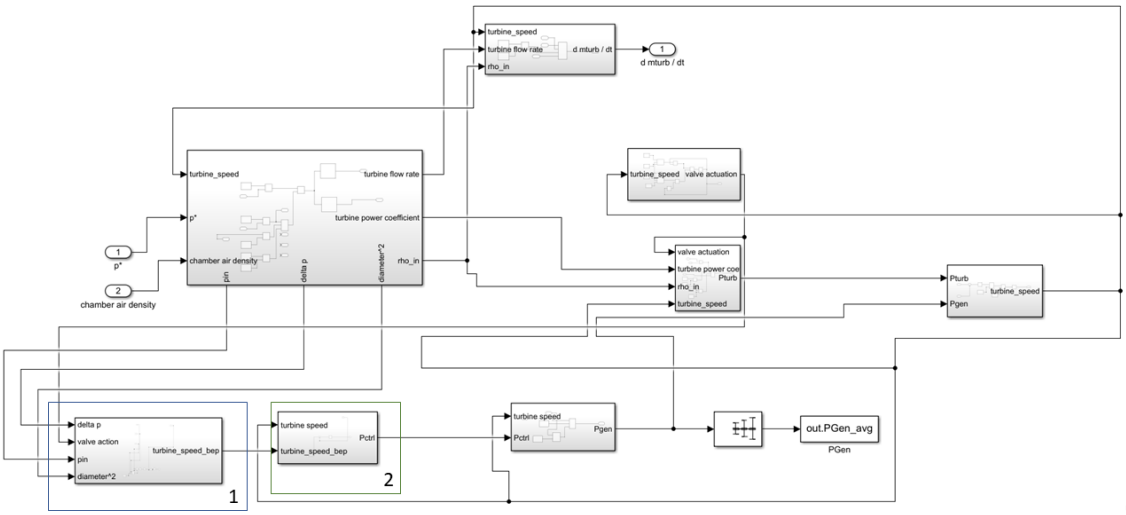

Figure 5.11: PTO model with an PID Controller

As shown in the Figure 5.12, which corresponds to the blue rectangle, at each time-step, a new Ω_{bep} is computed through the Equation 4.21

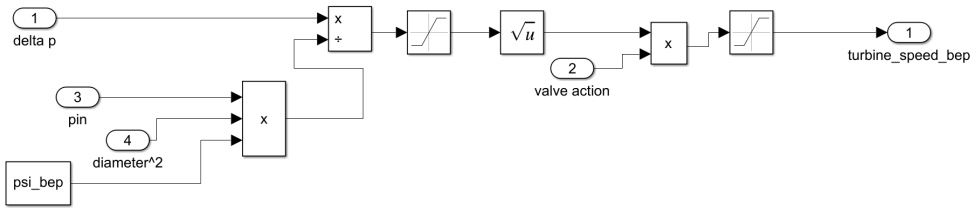

Figure 5.12: Computation of the needed turbine speed, Ω_{bep}

The classical PID model is used as demonstrated in the Figure 5.13, which corresponds to the green rectangle, still follows the generator power overload restriction as seen by the Equation 4.15.

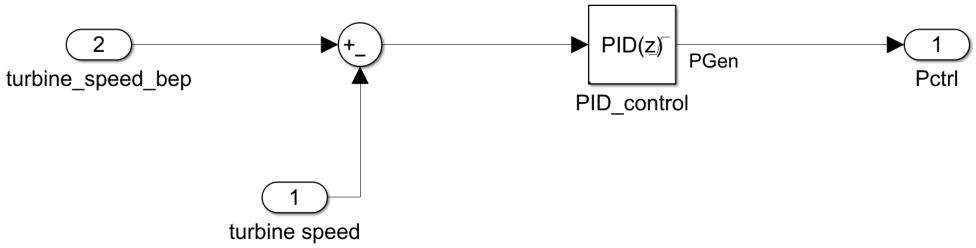

Figure 5.13: Simulink model of the PID Controller

All the remaining blocks are the same as in the model described in Section 5.2.

As mentioned in Section 4.2.2, the PID parameters for each sea state were computed using a PSO algorithm presented in the code block A.4, leading to the results shown in the following table 5.4:

Sea state	PID Parameters			
	P	I	D	N
1	40.07	-21.45	-24.44	2.31
2	21.51	-38.07	-11.91	2.22
3	1.58	-34.75	-14.35	2.41
4	2.18	-48.25	-6.83	3.12
5	48.31	-14.77	-48.73	2.43
6	23.12	-38.54	-50	3.68
7	47.8	-17.35	-43.12	2.32
8	48.1	-12.62	-45.12	2.12
9	13.18	-13.09	-47.21	2.47
10	10.11	-30.01	-46.61	2.18
11	23.67	-7.38	-38.12	3.24
12	12.68	-8.27	-26.97	0.93
13	19.12	-19.78	-8.13	1.97
14	38.87	-6.98	-38.17	3.04

Table 5.4: PID Parameters for each sea state

Chapter 6

Results

On this chapter, the results obtained with the above described models are detailed for the consequent analysis.

6.1 Optimised Parameters Control (OPC)

6.1.1 Statistical Results

As mentioned in chapter 5, the Simulink model was used to simulate the OWC response to different sea States. In this case, all simulations were made using a fixed time-step = 0.001 s for around 1500 s, and the chosen solver was the ode3 (Bogacki-Shampine).

In order to validate the data, the available wave power per meter is computed using Equation 5.2. As seen in Section 5.1, the OWC chamber has a width of $10m$. Therefore the maximum available wave power will result from the Equation 5.2 $\times$ the chamber width. This will be used as a comparison point to obtain the average OWC efficiency when using the average OWC Power for each sea state.

As mentioned in the previous chapters, the PSO algorithm uses the trained ANN to search for the most optimal control parameters a and b, as stated in the generator control Equation 4.14, which will bring the highest time average generated power, just as in the Matlab Script A.3. This result will be posteriorly compared with fixed control parameters obtained using a statistical analysis based on the probability of occurrence of the sea states as stated in [59]. The results are shown in the Table below 6.1:

Sea State	$P_{wave}(kW)$	$\overline{P_{OWC}}(kW)$		$\eta_{elec}(\%)$	
		Reference parameters	**Variable parameters**	**Reference parameters**	**Variable parameters**
1	32.56	20.93	23.12	64.28	70.99
2	52.71	21.53	24.86	40.85	47.16
3	62.01	21.29	22.67	34.33	36.56
4	67.6	16.78	18.31	24.82	27.08
5	84.7	13.631	16.07	16.09	18.97
6	113.66	12.87	14.43	11.32	12.7
7	146.29	12.95	14.54	8.85	9.94
8	209.29	13.27	15.01	6.34	7.17
9	338.08	15.96	17.93	4.72	5.3
10	474.94	17.63	19.83	3.71	4.17
11	794.81	20.47	22.83	2.58	2.87
12	1046.17	22.05	24.37	2.11	2.33
13	877.82	24.68	28.28	2.81	3.22
14	978.46	25.22	28.41	2.58	2.89

Table 6.1: Comparison between available wave power and the generated OWC power at both types of control

where P_{wave} is the available wave power, $\overline{P_{OWC}}$ is the average generated OWC power, which depends on which control is being used: fixed parameters (Reference) or using optimised parameters (Variable parameters). At last the η_{elec} is computed by dividing the $\overline{P_{OWC}}$ with the P_{wave}.

Average efficiency is also computed using a weighted average, $\overline{\eta_{elec}}$, which uses the probability of occurrence of each sea state. This way, a more accurate result can be withdrawn to how much the control has improved the OWC behaviour and if this type of control can be a viable option. The following Table 6.2 compares the OWC efficiency at both types of control:

$\overline{\eta_{elec}}$	
Reference parameters	**Optimised Parameters**
17.68	19.79

Table 6.2: OWC overall electric efficiency

The following Table 6.3 compares how much improvement the optimal parameter control can bring in this model against fixed parameters, where the average improvement was also computed using a weighted average for each sea state, just like in Table 6.2:

Sea State	Optimal Control Improvement(%)
1	10.45
2	15.47
3	6.48
4	9.12
5	17.8
6	12.12
7	12.28
8	13.11
9	12.34
10	12.48
11	11.53
12	10.52
13	14.58
14	12.64
Average Improvement	12.48

Table 6.3: Comparison between generated OWC power at both types of control

6.1.2 Hydrodynamic, Aerodynamics and PTO Results

To further comprehend the numerical results in the previous subsection, some visible results were taken to help explain how the entire system works and where the control is being applied. The following Figures were taken from simulations with a time span of 500 *s* and a time-step of 0.001 *s* to enhance the details of the OWC dynamics and to ease its analysis.

In order to analyse how the OWC responds to different available wave power and if a resonate state can be achieved, three different sea states were chosen to analyse further:

- sea state 2 (low available wave power)
- sea state 8 (medium available wave power)
- sea state 14 (high available wave power)

Starting with the imaginary piston position, it is crucial in order to understand how the piston position correlates with the turbine pressure head. The following Figure 6.1 shows how it varies depending on each chosen sea state:

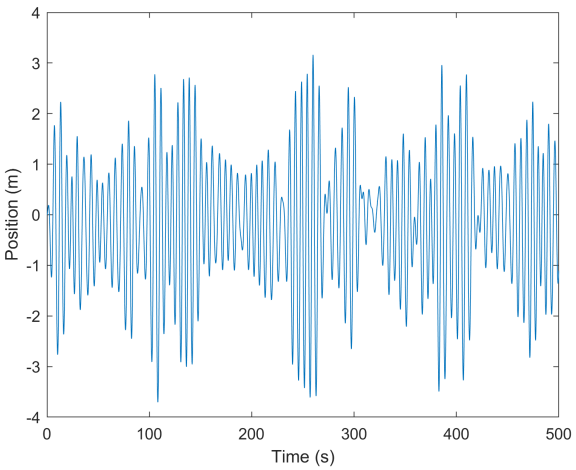

(a) Piston Position at Sea State 2

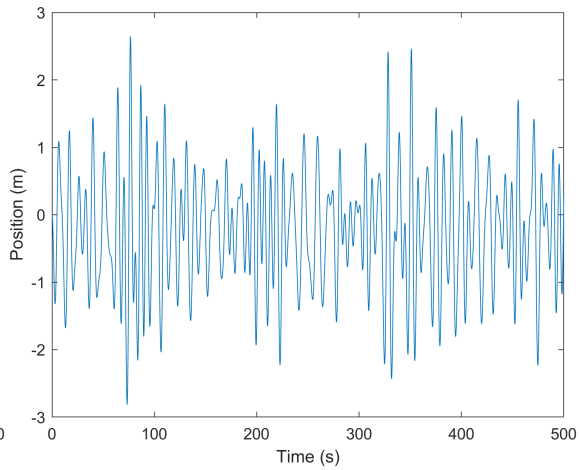

(b) Piston Position at Sea State 8

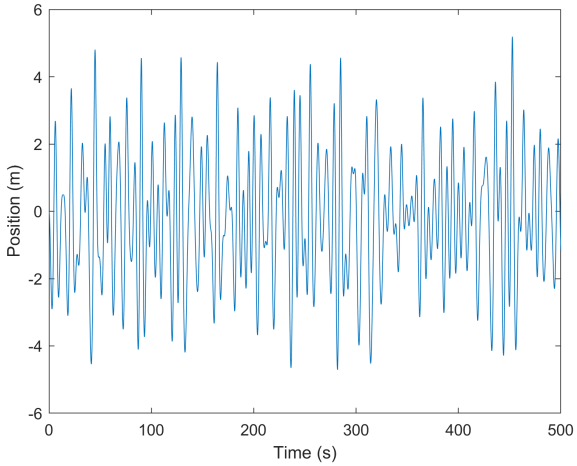

(c) Piston Position at Sea State 14

Figure 6.1: Piston Position at sea state 2,8 and 14

Secondly, the dimensionless turbine pressure head is also essential to analyse since the turbine characteristics can be computed using the curves 4.2, and therefore it allows a higher notion of how to interpret the results. The following Figure 6.2 shows how the pressure head varies depending on each chosen sea state:

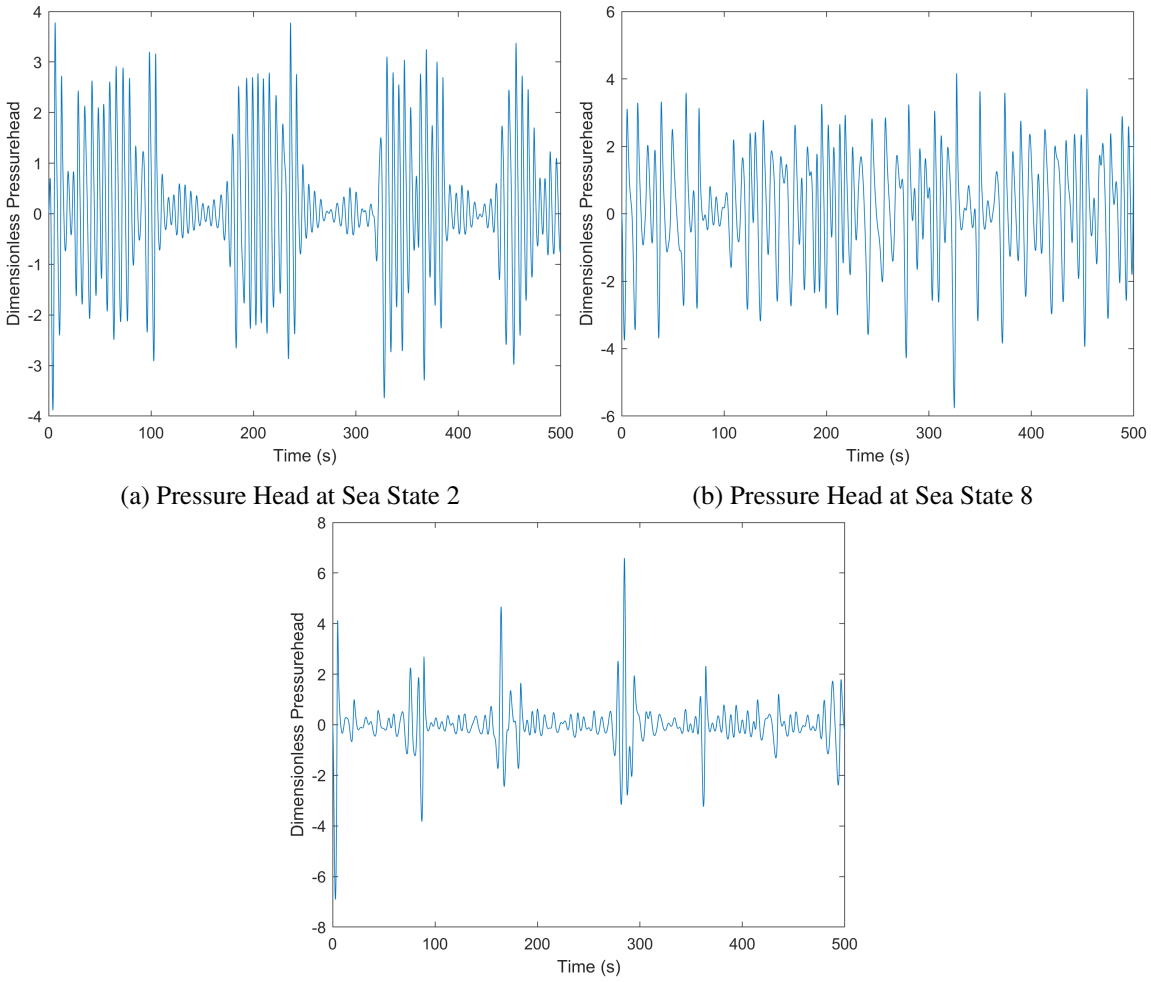

(a) Pressure Head at Sea State 2

(b) Pressure Head at Sea State 8

(c) Pressure Head at Sea State 14

Figure 6.2: Pressure Head at sea state 2,8 and 14

In order to understand and visualise how the generated power is produced, a comparison between how the turbine power develops along the time span and how the generator reacts, following the Equation 4.14.This relation is shown in the following Figure 6.3:

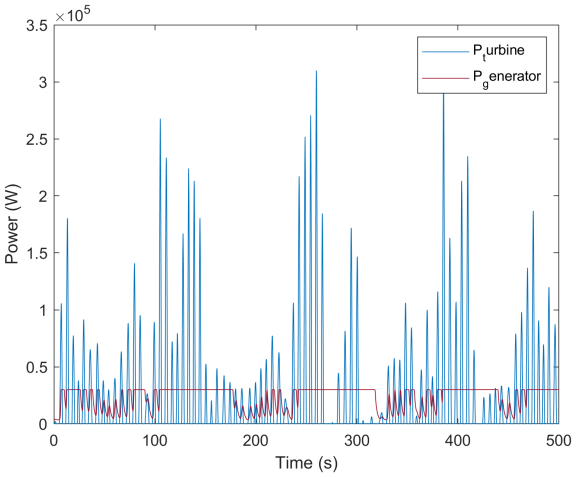

(a) Turbine and Generated Power at Sea State 2 using the optimised parameters

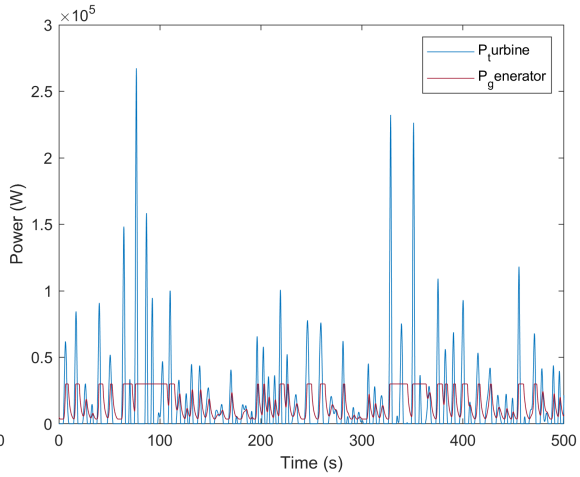

(b) Turbine and Generated Power at Sea State 8 using the optimised parameters

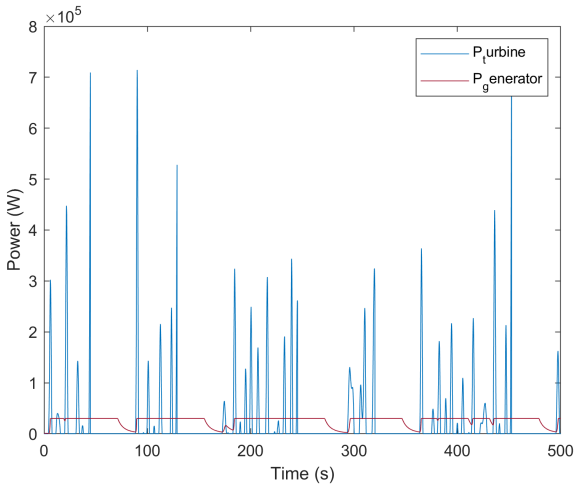

(c) Turbine and Generated Power at Sea State 14 using the optimised parameters

Figure 6.3: Turbine and Generated Power at the sea state 2,8 and 14 using the optimised control parameters

Lastly, the high-speed safety valve also acts differently depending on how turbine rotational speed that instant when analysing together with the following the Equation 4.18. It also allows the user to understand when this HSSV happens and the effect that it has when compared with the previous Figures. This HSSV actuation can be seen by the following Figure 6.4c:

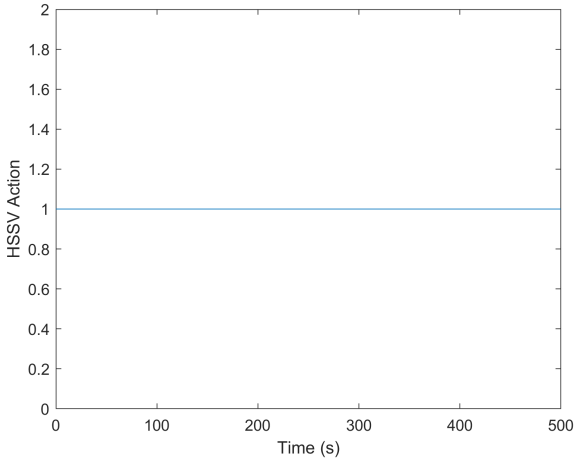

(a) HSSV actuation at Sea State 2 using the optimised parameters

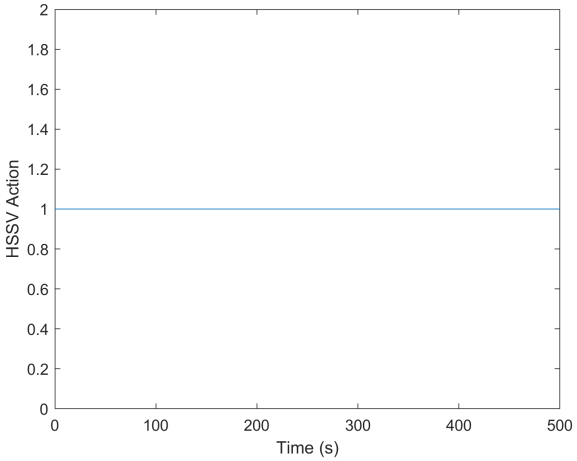

(b) HSSV actuation at Sea State 8 using the optimised parameters

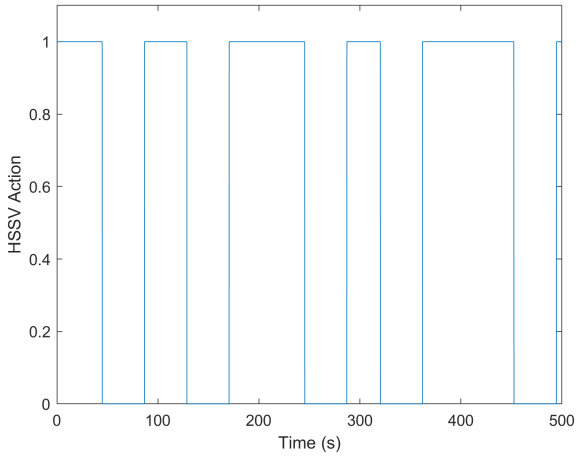

(c) HSSV actuation at Sea State 14 using the optimised parameters

Figure 6.4: HSSV actuation at sea state 2,8 and 14 with optimised control parameters

It should be noted that when the HSSV Actuation value is equal to zero, the HSSV is opened (safe mode), and if it equals to one, it's closed (normal mode).

6.2 PID Control

6.2.1 Statistical Results

As in the previous results, the Simulink model was also used to test this type of control. All simulations were made using a fixed time-step = 0.001 s for around 1500 s, and the chosen solver was the ode3.

This PID control was compared with the available wave power plant and with the reference control law 5.2 to validate the data and to check if any improvement was made in the energy capture.

As mentioned in Section 5.4, there is a set of optimised PID parameters for each sea state, which will bring the turbine to its most efficient point through the error between the optimal and the actual rotational speed. It should also be noted that the optimal turbine speed is not a constant value, as it follows the Relation 4.21. The results are shown in the Table bellow 6.4:

Sea State	$P_{wave}(kW)$	$\overline{P_{OWC}}(kW)$		$\eta_{elec}(\%)$	
		Reference	**PID Control**	**Reference**	**PID Control**
1	32.56	20.93	21.04	64.28	64.63
2	52.71	21.53	22.31	40.85	42.33
3	62.01	21.29	21.51	34.33	34.69
4	67.6	16.78	17.65	24.82	26.11
5	84.7	13.63	14.21	16.09	16.78
6	113.66	12.87	13.27	11.32	11.67
7	146.29	12.95	13.69	8.85	9.36
8	209.29	13.27	13.98	6.34	6.68
9	338.08	15.96	17.09	4.72	5.06
10	474.94	17.63	19.48	3.71	4.10
11	794.81	20.47	21.68	2.58	2.73
12	1046.17	22.05	23.83	2.11	2.28
13	877.82	24.68	27.05	2.81	3.08
14	978.46	25.22	27.89	2.58	2.85

Table 6.4: Comparison between available wave power and the generated OWC power at both types of control (PID and Ref)

where the $\overline{P_{OWC}}$ is the average potency which depends on which control is being used: fixed parameters (Reference) or by using a PID. At last the η_{elec} is computed by dividing the $\overline{P_{OWC}}$ by P_{wave}.

In the same way, as done before, the average efficiency, $\overline{\eta_{elec}}$, is also computed using a weighted average concerning the probability of occurrence of each sea state, as shown in the below Table 6.5:

$\overline{\eta_{elec}}$	
Reference parameters	**PID control**
17.68	18.26

Table 6.5: OWC overall electric efficiency

The following Table 6.6 compares how much improvement the PID control can bring in this model against fixed parameters, and the average improvement was calculated the same way as the previous Section Table 6.3:

Sea State	**PID Control Improvement(%)**
1	0.53
2	3.62
3	1.03
4	5.18
5	4.26
6	3.1
7	5.71
8	5.35
9	7.08
10	10.49
11	5.91
12	8.07
13	9.6
14	10.58
Average Improvement	4.58

Table 6.6: Comparison between generated OWC power for both types of control (PID and Reference)

6.2.2 PTO Results

Like in the variable parameters control results, to further comprehend how the PID control affects the OWC system, time-series graphics were produced to analyse the different behaviour further. The following Figures were also taken from simulations with a time span of 500 s and a time-step of 0.001 s. It should be noted that the imaginary piston position and pressure head figures were not necessary to repeat since their behaviour will be similar. Just analysing the rotational speed, which brings the turbine to its highest efficiency point and the actual turbine speed is enough to understand and make conclusions about the PID actuation in this model.

Starting with the HSSV actuation, the following Figure 6.5 shows how it is applied throughout different sea states:

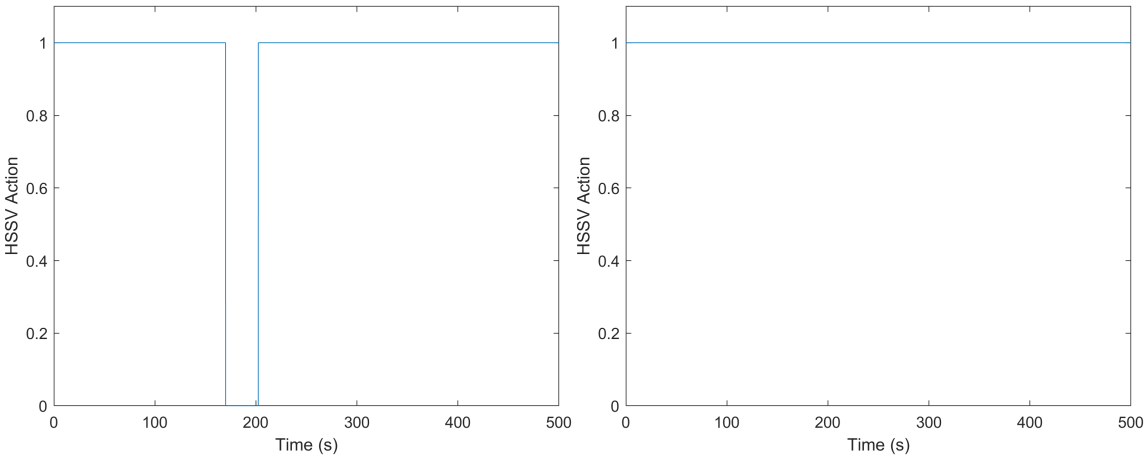

(a) HSSV actuation at Sea State 2 using a PID

(b) HSSV actuation at Sea State 8 using a PID

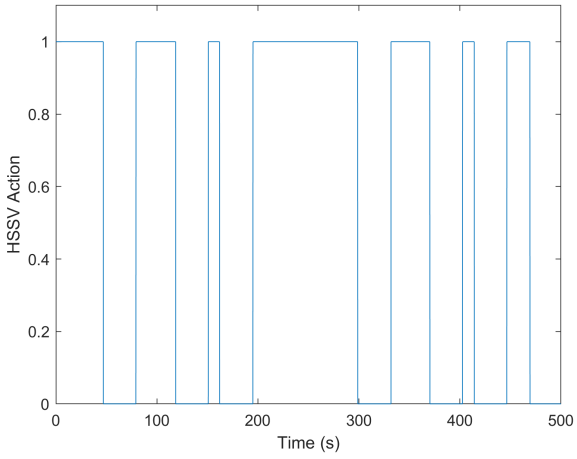

(c) HSSV actuation at Sea State 14 using a PID

Figure 6.5: HSSV actuation at sea state 2,8 and 14 for PID Control

Secondly, as mentioned in Section 4.2.2, the error produced is between the most efficient rotational speed and the actual rotational speed that generates the PID response, which will be the instantaneous generator electromagnetic power imposed to control the rotational speed (P_{gen}). Therefore, an analysis of how the Ω_{bep} changes between each sea state and its magnitude is essential, just as shown in the Figure 6.6:

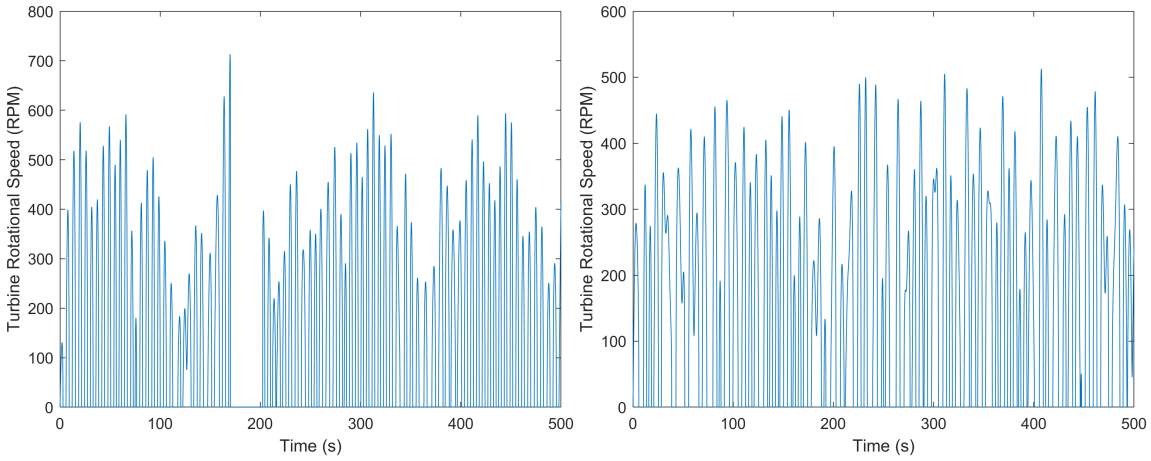

(a) Rotational Speed at the best efficiency for the Sea State 2

(b) Rotational Speed at the best efficiency for the Sea State 8

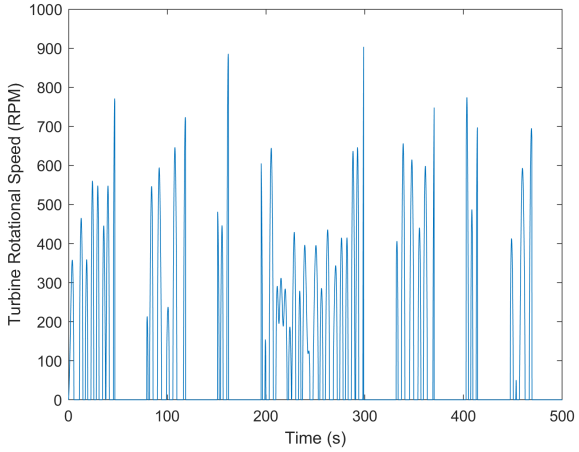

(c) Rotational Speed at the best efficiency for the Sea State 14

Figure 6.6: Rotational Speed at the best efficiency for the sea states 2,8 and 14 using PID control

Finally, like in the previously tested control, visualising the available power at the turbine and the generated power can help understand how the control system is taking advantage of it and how the actual rotational turbine speed depends on both values, as seen by the Equation 4.7, therefore it is fundamental to analyse both values. The following Figure 6.7 shows the different behaviour in those chosen sea states.

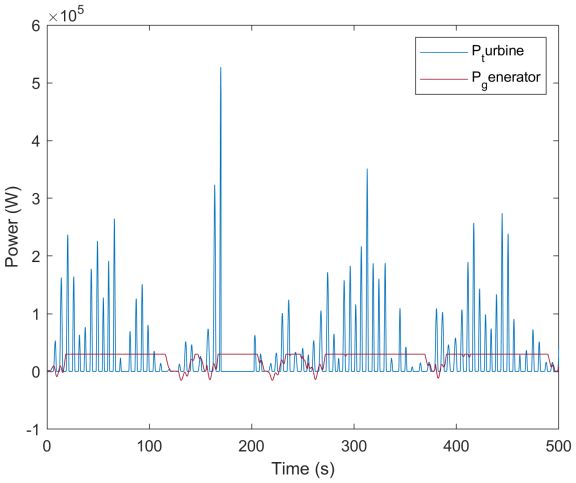

(a) Turbine and Generated Power at Sea State 2 using a PID

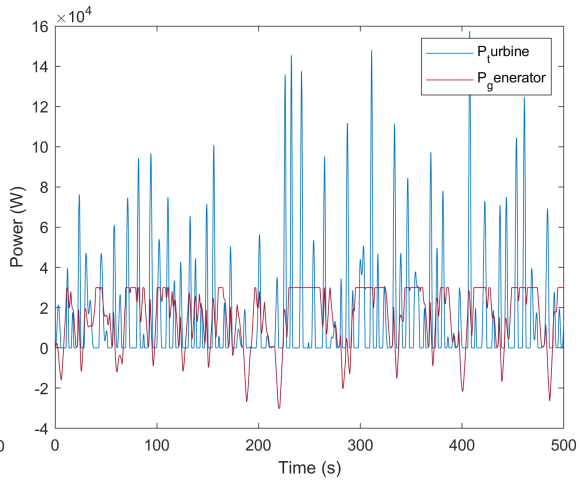

(b) Turbine and Generated Power at Sea State 8 using a PID

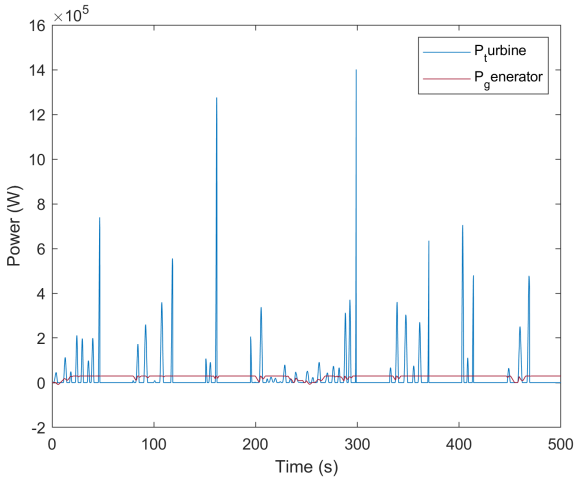

(c) Turbine and Generated Power at Sea State 14 using a PID

Figure 6.7: Turbine and Generated Power at the sea state 2,8 and 14 in a PID Control

6.3 Comparison between PID Control and Optimised Parameters Control

To deduce which type of control is more effective and which situation can be more useful than the other, a comparison between the average generated power is made since this study's objective is to optimise the output power of the OWC. The following Table 6.7 highlights this comparison:

Sea state	$\overline{P_{OWC}}(kW)$		$\frac{OPC-PID}{PID}$ (%)
	Optimised Parameters Control (OPC)	**PID Control**	
1	23.12	21.04	9.86
2	24.86	22.31	11.41
3	22.86	21.51	5.4
4	18.31	17.65	3.72
5	16.07	14.21	13.1
6	14.43	13.27	8.81
7	14.54	13.69	6.13
8	15.01	13.98	7.34
9	17.93	17.09	4.85
10	19.83	19.48	1.77
11	22.83	21.68	5.3
12	24.37	23.83	2.29
13	28.28	27.05	4.62
14	28.41	27.89	1.42

Table 6.7: Comparison between the average generated power using Optimised Parameters Control (OPC) or PID Control

It should also be noted that to justify different advantages, the results from previous sections will also be used, particularly the PTO Results of each Section 6.1.2 and 6.2.2.

Chapter 7

Results Analysis

7.1 Optimised Parameters Control (OPC)

According to Table 6.1, the OWC efficiency relative to the available wave power is acceptable in the first five sea states. From then on, the OWC cannot keep up with the available power since the turbine/generator cannot have the rotational speed pass a specific limit according to the Equation 4.18, and can not overload the generator. It also cannot generate power higher than its rater power. Another problem can be that the selected architecture does not have the best response to certain sea states. As seen in Table 6.2, an overall 2.11% was improved concerning the reference control law.

Comparing only what the OWC with both types of control can improve against the available power can give the wrong idea of how much using optimised parameters can improve the OWC response against the fixed values, as seen by the low improvement in Table 6.2. Therefore Table 6.3 only compares how much progress was made in the capture efficiency at each sea state, not accounting for how much Wave power was available. This led to an overall improvement of $12,48\%$, where the control law allowed the generator to perform at its rated power for an extended period, which could not be achieved with a Wells turbine. The result was already anticipated since the algorithm utilised the best parameters for each sea state so that, at the very least, the same reference result would be obtained.

Taking into account the Figures 6.1, 6.2, 6.4, 6.3 and considering the sea state 14, and even though there are instances where the HSSV actuates, just as in Figure 6.4c, due to the actuation of the control explicit in the Equations 4.18 and 4.19. This will decrease the rotational speed, and the generated power will stop being the same as the rated power after a while. In this case, as clearly noted in Figure 6.2c, these pressure head spikes correspond to the time intervals where the HSSV is open. As seen in Figure 4.2, high-pressure values correspond to high turbine power coefficients, making the turbine accelerate until the HSSV needs to actuate again. This will make the generated power constant at the rated power following the Equation 4.14 when the valve is open, and for a while, the rotational speed decreases following the valve closure, as seen in Figure 6.3c. Finally,

as seen in Figure 6.1c, this sea state will lead to the highest OWC oscillations, which proves the high turbine pressure head values.

Theoretically comparing sea state 2 and sea state 8, the OWC would produce more energy since there is also more wave power available, as demonstrated in Table 6.1. Still, this will not happen in practice for this architecture and biradial turbine. This is proved by taking note of the Figure 6.1a and 6.1b, where in sea state 2, the imaginary piston in the chamber reaches a higher max value than the one in sea state 8, and also by taking a closer look at the Figures 6.2a and 6.2b where in the sea state 2 also reaches a higher turbine pressure head, leading to a higher power coefficient. These higher values can be explained because, according to [59], the OWC model taken from Mutriki OWC-breakwater has a resonance period around 6 s, which is around the effective wave period of the sea state 2, which will cause an increase in the oscillations inside the OWC, leading to a higher energy capture. This type of turbine also aids this type of behaviour because, unlike the Wells turbine, which loses most of its efficiency at a high turbine pressure head. The biradial turbine assumes a nearly constant efficiency at that higher range of values. Therefore, a higher pressure head will not always be negative, only if it leads to the HSSV actuation.

7.2 PID Control

Taking into account the Table 6.4, where the PID control and the reference control (fixed control parameters) are compared with the available wave power in the OWC, an overall electric efficiency improvement of around 1%, as seen in Table 6.5, therefore it should be more appropriate to compare only the reference control with the PID control as seen in the Table 6.6. This Table exhibits that the PID control shines in higher sea states. Still, for the considered sea states and their frequency of occurrence, this improved efficiency in higher sea states will not bring the needed boost for the overall OWC efficiency, making it seems that the PID control is not a very viable option since its implementation is more complex than a simple control rule used in the reference control law. This type of control improved the efficiency by $4,58\%$ in relation to the fixed control law used.

Highlighting the sea state 2, the PID control causes the action of the HSSV, as seen in Figure 6.5a, due to the rotational speed at the best efficiency at that instant, as seen in Figure 6.6a, surpasses the max allowed rotational speed of 640 *RPM* computed by the Equation 4.18. The PID actuates following the current error to maximise the turbine efficiency. There may be instances where the best efficiency rotational speed may surpass the limit imposed to avoid the flow comprehensibility effects, which are not accounted for in the curves illustrated in Figure 4.2 since it depends on the turbine blades length. As mentioned before, the sea state 2 is at the resonance frequency of this OWC, which causes a higher turbine rotational speed. It can also be seen by the Figure 6.7a that in some instances, in order to achieve a faster rotational speed acceleration, following the Equation 4.7, the generator is shown to produce negative values, which means that the generator is behaving as a motor, consuming power from the grid. All this will lead to efficiency improvement, but not very notorious.

As for sea state 8, it has a similar behaviour as the previously discussed sea stat, but as the available pneumatic power is lower due to not being at a resonance state, the most efficient rotational speed does not achieve a value which will lead to the HSSV actuation. The lower available turbine power makes the generator behave like a motor at a higher frequency and amplitude, as seen by Figure 6.7b, to achieve a higher rotational acceleration. This does not happen as much in the previous sea state since the P_{ctrl} does not need to compensate for the lower turbine power, following the Equation 4.7.

Finally, sea state 14, among the other sea states, has the highest efficiency improvement since the high available turbine power does not lead to a motor behaviour by the generator. Therefore, there will not be a decrease in the average generated power, as in the previously stated sea states. The problem starts with the HSSV actuation, where the most efficient rotational speed is, most of the time, higher than its imposed limit, leading to the frequent HSSV actuation, as seen in Figure 6.5c. It should be noted that the instances where the most efficient rotational speed is at zero are the instances where the HSSV is closed, as seen by comparing the Figures 6.5c and 6.6c. Following Figure 6.7c, when the valve actuates (periods where the turbine power is at zero), the generator stays for a while at rated power to provide a higher deceleration, as seen by the Equation 4.7.

7.3 Comparation between PID Control and Optimised Parameters Control

A final comparison between both studied types of control was made in Table 6.7. From there, we can deduce that the OPC control achieves a better overall result in all cases, especially at a lower energy sea state, where we have a peak difference of around $13,10\%$. After analysing how the system reacts to each type of control, these results are already expected. The PID has demonstrated before brought several issues:

- brought the turbine rotational speed faster to the limit imposed by the control law 4.18, which affected the generated power negatively.
- in lower energetic sea states, the generator had to work as a motor to speed up the turbine rotational speed in order to achieve the desired one.

As seen in Table 6.7, the most significant difference between the average generated power of both types of control is highlighted in the lower sea states, where the resonance behaviour occurred, so the HSSV actuation started to happen in the PID control, as mentioned before, and there were also some instances where energy was taken from the grid for the generator to act as a motor. In the more medium energetic sea states, the main problem was power loss due to the energy taken from the grid, and in the highest energetic sea states, the problem was the HSSV actuation being more frequent. It should also be noted that the HSSV actuation is assumed to be instantaneous, which is impossible in a real environment.

Even though the PID brought worse results, it should be discarded as a control option since training the artificial neural network is more time-consuming to obtain good results, whereas finding the optimal PID parameters is faster. Therefore, a PID controller can bring a better initial result in a real-life situation, whereas the Ann network would take longer to produce valid results.

Chapter 8

Conclusions and Future Work

Although the Oscillating water column is one of the most developed systems for wave energy, it still can't compete with the renewable energy like solar and wind power. To overcome this problem, turbine/generator set control algorithms with the aid of artificial intelligence were developed. Therefore two different case studies were done to study its viability: PID Controller tuned using a PSO algorithm and an ANN with a PSO algorithm which finds the optimal generator control parameter. These two types of control brought an average improvement of around 4.58% and 12.48%, respectively.

The Optimised Parameters Control (OPC) can converge using the ANN to the optimal control parameters. This ANN can map the non-linear relation between the mean generated power with the wave energy period (T_e), the significant wave height (H_s) and the generator control parameters (a and b). A global optimisation algorithm, in this case, the Particle swarm optimisation (PSO), is used to determine the control parameters that will be used at each time horizon, using the known significant wave height and energy wave period.

The PID Control is used to make the turbine rotational speed at that instance, approach a value that brings the turbine to its best efficiency point. This best efficiency point is not a fixed value since it depends on the stagnation pressure head (Δp) and the turbine inlet density (ρ_{in}), as seen by the Equation 4.21. The downside of this type of control is that in the PID, the generator will act as a motor for a certain period to maintain a certain rotational speed. This will make this type of control slightly worst than the previously mentioned, as seen by Table 6.7, where the OPC control had a significantly better performance in the earlier sea states since the motor behaviour tended to happen in lower energy sea states.

It should also be noted that this study was made in a near-perfect environment. The high-speed safety valve actuation was considered instantaneous, which is impossible since there will be a delay imposed by receiving the order to actuate and the time it takes to fully close or open. The OWC state is also assumed to be in perfect conditions, without any wear. As mentioned in Chapter 5, at each time horizon, the sea state should be known as a priory, and in this work, it is assumed to be known. However, in reality, knowing precisely what the next sea state will be, needs to be done through predictions. At last, the results shown in the Chapter 6 were done using

a fully trained neural network and a tuned PID for each sea state, whereas, in reality, this type of training and tuning would take a longer time to achieve and probably wouldn't reach such degree.

In future work, some of these preciously mentioned issues could be solved. Just as, instead of knowing precisely the future sea state, a prediction should be made, for example, by using a grey model or an ANN. Another interesting approach would be, instead of having a fully trained ANN for mapping the non-linear relationship discussed above, a fully untrained ANN should be used, and the training should occur incrementally with the help of a PSO algorithm. This way, a real behaviour will be tested since, in reality, the OWC initially wouldn't have any collected data to train its neural network, therefore testing how much time it would take and how the system would respond until the ANN is fully trained or at an optimal state, would be useful. At last, the PID control could be done using an Adaptive PID Controller based on a Q-learning Algorithm, which uses trained Q-tables to change the gains of linear PID controllers according to the state of the system (current sea state) during the control process.

References

[1] Why onshore/nearshore? - eco wave power. URL: https://www.ecowavepower.com/our-technology/why-onshore-nearshore/.

[2] OpenLearn. Wave energy technologies, 2022. URL: https://www.open.edu/openlearn/mod/oucontent/view.php?id=73764&section=4.

[3] Arqam Ilyas, Syed A.R. Kashif, Muhammad A. Saqib, and Muhammad M. Asad. Wave electrical energy systems: Implementation, challenges and environmental issues, 2014. doi:10.1016/j.rser.2014.07.085.

[4] António F.O. Falcão, João C.C. Henriques, and Luís M.C. Gato. Self-rectifying air turbines for wave energy conversion: A comparative analysis, 2018. doi:10.1016/j.rser.2018.04.019.

[5] António F.O. Falcão and João C.C. Henriques. Oscillating-water-column wave energy converters and air turbines: A review, 2016. doi:10.1016/j.renene.2015.07.086.

[6] Markel Penalba and John V. Ringwood. A review of wave-to-wire models for wave energy converters, 2016. doi:10.3390/en9070506.

[7] J. C.C. Henriques, W. Sheng, A. F.O. Falcão, and L. M.C. Gato. A comparison of biradial and wells air turbines on the mutriku breakwater owc wave power plant. volume 10, 2017. doi:10.1115/OMAE2017-62651.

[8] S. Astariz, A. Vazquez, and G. Iglesias. Evaluation and comparison of the levelized cost of tidal, wave, and offshore wind energy. *Journal of Renewable and Sustainable Energy*, 7, 2015. doi:10.1063/1.4932154.

[9] Andreas Uihlein and Davide Magagna. Wave and tidal current energy - a review of the current state of research beyond technology, 2016. doi:10.1016/j.rser.2015.12.284.

[10] Nicola Delmonte, Davide Barater, Francesco Giuliani, Paolo Cova, and Giampaolo Buticchi. Review of oscillating water column converters, 2016. doi:10.1109/TIA.2015.2490629.

[11] T. V. Heath. A review of oscillating water columns. volume 370, 2012. doi:10.1098/rsta.2011.0164.

[12] Robin Pelc and Rod M. Fujita. Renewable energy from the ocean. *Marine Policy*, 26, 2002. doi:10.1016/S0308-597X(02)00045-3.

[13] Paul A. Lynn. *Electricity from wave and tide: An introduction to marine energy*. 2013. doi:10.1002/9781118701669.

[14] João Rocha, Tiago Abreu, and Carlos Felgueiras. Evaluation of potential tidal impoundment energy systems in ria de aveiro, portugal. *Energy Reports*, 6, 2020. doi:10.1016/j.egyr.2020.11.115.

[15] Johannes Falnes. A review of wave-energy extraction, 2007. doi:10.1016/j.marstruc.2007.09.001.

[16] Alain Clément, Pat McCullen, António Falcão, Antonio Fiorentino, Fred Gardner, Karin Hammarlund, George Lemonis, Tony Lewis, Kim Nielsen, Simona Petroncini, M. Teresa Pontes, Phillippe Schild, Bengt Olov Sjöström, Hans Christian Sørensen, and Tom Thorpe. Wave energy in europe: Current status and perspectives, 2002. doi:10.1016/S1364-0321(02)00009-6.

[17] B. Drew, A. R. Plummer, and M. N. Sahinkaya. A review of wave energy converter technology, 2009. doi:10.1243/09576509JPE782.

[18] John D. Isaacs and Richard J. Seymour. The ocean as a power resource. *International Journal of Environmental Studies*, 4, 1973. doi:10.1080/00207237308709563.

[19] Gunnar Mørk, Stephen Barstow, Alina Kabuth, and M. Teresa Pontes. Assessing the global wave energy potential. volume 3, 2010. doi:10.1115/OMAE2010-20473.

[20] D. Mawooa, L. Latchoomun, R. G. Kaully, and Krishna Busawon. An overview of wave energy technologies in the mauritian context. 2019. doi:10.1109/EFEA.2018.8617087.

[21] Balazs Czech and Pavol Bauer. Wave energy converter concepts : Design challenges and classification, 2012. doi:10.1109/MIE.2012.2193290.

[22] Dongsheng Qiao, Rizwan Haider, Jun Yan, Dezhi Ning, and Binbin Li. Review of wave energy converter and design of mooring system, 2020. doi:10.3390/su12198251.

[23] Mohammed Faizal, M Rafiuddin Ahmed, and Young-Ho Lee. A design outline for floating point absorber wave energy converters. 2014. URL: http://dx.doi.org/10.1155/2014/846097, doi:10.1155/2014/846097.

[24] I. López, B. Pereiras, F. Castro, and G. Iglesias. Performance of owc wave energy converters: Influence of turbine damping and tidal variability. *International Journal of Energy Research*, 39, 2015. doi:10.1002/er.3239.

[25] Af De O Falcão. The shoreline owc wave power plant at the azores. *Proceedings of the fourth European wave energy conference*, 2000.

[26] António F.O. Falcão, António J.N.A. Sarmento, Luís M.C. Gato, and Ana Brito-Melo. The pico owc wave power plant: Its lifetime from conception to closure 1986–2018. *Applied Ocean Research*, 98, 2020. doi:10.1016/j.apor.2020.102104.

[27] Cuan B. Boake, Trevor J.T. Whittaker, Matt Folley, and Hamish Ellen. Overview and initial operational experience of the limpet wave energy plant. volume 12, 2002.

[28] Y Torre-Enciso, I Ortubia, L I López de Aguileta, and J Marqués. Mutriku wave power plant: from the thinking out to the reality. *8th European Wave and Tidal Energy Conference (EWTEC 2009)*, 2009.

[29] Gabriel Ibarra-Berastegi, Jon Sáenz, Alain Ulazia, Paula Serras, Ganix Esnaola, and Carlos Garcia-Soto. Electricity production, capacity factor, and plant efficiency index at the mutriku wave farm (2014–2016). *Ocean Engineering*, 147, 2018. doi:10.1016/j.oceaneng.2017.10.018.

[30] Yoshio Masuda, Tetuo Yamazaki, Yoshiyuki Outa, and Michael E. McCormick. Study of backward bent duct buoy. 1987. doi:10.1109/oceans.1987.1160750.

[31] Wanan Sheng. Power performance of bbdb owc wave energy converters. *Renewable Energy*, 132, 2019. doi:10.1016/j.renene.2018.07.111.

[32] Luca Martinelli, Paolo Pezzutto, and Piero Ruol. Experimentally based model to size the geometry of a new owc device, with reference to the mediterranean sea wave environment. *Energies*, 6, 2013. doi:10.3390/en6094696.

[33] A. F O Falcao and L. M C Gato. *Air turbines, in: A. Sayigh (Ed.), Comprehensive Renewable Energy,*, volume 8. 2012.

[34] R Starzmann, T Zhu, C Moisel, and Th Carolus. Aero-acoustic analysis of the wells turbine with guide vanes. *4th International Conference on Ocean Energy*, 1, 2012.

[35] T. Karthikeyan, Abdus Samad, and Rameez Badhurshah. Review of air turbines for wave energy conversion. 2014. doi:10.1109/ICRESE.2013.6927812.

[36] T. Setoguchi, S. Santhakumar, H. Maeda, M. Takao, and K. Kaneko. A review of impulse turbines for wave energy conversion. *Renewable Energy*, 23, 2001. doi:10.1016/S0960-1481(00)00175-0.

[37] H. Maeda, S. Santhakumar, T. Setoguchi, M. Takao, Y. Kinoue, and K. Kaneko. Performance of an impulse turbine with fixed guide vanes for wave power conversion. *Renewable Energy*, 17, 1999. doi:10.1016/S0960-1481(98)00771-X.

[38] A. A.D. Carrelhas, L. M.C. Gato, J. C.C. Henriques, A. F.O. Falcão, and J. Varandas. Test results of a 30FIX ME!!!!kw self-rectifying biradial air turbine-generator prototype. *Renewable and Sustainable Energy Reviews*, 109, 2019. doi:10.1016/j.rser.2019.04.008.

[39] A. F.O. Falcão, L. M.C. Gato, and E. P.A.S. Nunes. A novel radial self-rectifying air turbine for use in wave energy converters. *Renewable Energy*, 50, 2013. doi:10.1016/j.renene.2012.06.050.

[40] John V. Ringwood, Giorgio Bacelli, and Francesco Fusco. Energy-maximizing control of wave-energy converters: The development of control system technology to optimize their operation. *IEEE Control Systems*, 34, 2014. doi:10.1109/MCS.2014.2333253.

[41] François Xavier Faÿ, João C. Henriques, James Kelly, Markus Mueller, Moahammad Abusara, Wanan Sheng, and Marga Marcos. Comparative assessment of control strategies for the biradial turbine in the mutriku owc plant. *Renewable Energy*, 146, 2020. doi:10.1016/j.renene.2019.08.074.

[42] A. F.de O. Falcão. Control of an oscillating-water-column wave power plant for maximum energy production. *Applied Ocean Research*, 24, 2002. doi:10.1016/S0141-1187(02)00021-4.

[43] Jon Lekube, Aitor J. Garrido, and Izaskun Garrido. Rotational speed optimization in oscillating water column wave power plants based on maximum power point tracking. *IEEE Transactions on Automation Science and Engineering*, 14, 2017. doi:10.1109/TASE.2016.2596579.

[44] Sunil Kumar Mishra, Shubhi Purwar, and Nand Kishor. Fuzzy logic control of owc wave energy plant for preventing wells turbine stalling. 2017. doi:10.1109/POWERI.2016.8077219.

[45] M. Amundarain Ormaza, M. Alberdi Goitia, A. J. Garrido Hernández, and I. Garrido Hernández. Neural control of the wells turbine-generator module. 2009. doi:10.1109/CDC.2009.5400638.

[46] Hoai-Nam Nguyen and Paolino Tona. Continuously adaptive pi-control of wave energy converters under irregular sea-state conditions. *Proceedings of the 12th European Wave and Tidal Energy Conference. Cork, Ireland*, 2017.

[47] Enrique Vidal Sanchez, Rico Hjerm Hansen, and Morten Mejlhede Kramer. Control performance assessment and design of optimal control to harvest ocean energy. *IEEE Journal of Oceanic Engineering*, 40, 2015. doi:10.1109/JOE.2013.2294386.

[48] Sunil Kumar Mishra, Shubhi Purwar, and Nand Kishor. Air flow control of owc wave power plants using fopid controller. 2015. doi:10.1109/CCA.2015.7320825.

[49] Aleksei Tepljakov, Baris Baykant Alagoz, Celaleddin Yeroglu, Emmanuel Gonzalez, S. Hassan HosseinNia, and Eduard Petlenkov. Fopid controllers and their industrial applications: A survey of recent results 1. volume 51, 2018. doi:10.1016/j.ifacol.2018.06.014.

[50] A. F.de O. Falcao, L. C. Vieira, P. A.P. Justino, and J. M.C.S. André. By-pass air-valve control of an owc wave power plant. *Journal of Offshore Mechanics and Arctic Engineering*, 125, 2003. doi:10.1115/1.1576815.

[51] K Budal and J Falnes. Interacting point absorbers with controlled motion, 1980.

[52] A. Babarit and A. H. Clément. Optimal latching control of a wave energy device in regular and irregular waves. *Applied Ocean Research*, 28, 2006. doi:10.1016/j.apor.2006.05.002.

[53] J. C.C. Henriques, L. M.C. Gato, A. F.O. Falcão, E. Robles, and F. X. Faÿ. Latching control of a floating oscillating-water-column wave energy converter. *Renewable Energy*, 90, 2016. doi:10.1016/j.renene.2015.12.065.

[54] Liang Li, Hongdong Wang, and Yan Gao. Development of a real-time latching control algorithm based on wave force prediction. *IEEE Journal of Oceanic Engineering*, 46, 2021. doi:10.1109/JOE.2020.2989657.

[55] D. Q. Truong and K. K. Ahn. Wave prediction based on a modified grey model mgm(1,1) for real-time control of wave energy converters in irregular waves. *Renewable Energy*, 43, 2012. doi:10.1016/j.renene.2011.11.047.

[56] Liang Li. *The Development of a Real-time Wave Energy Device Control Algorithm Based on Artificial Neural Network*. PhD thesis, University of Strathclyde, 2019.

[57] F. Saupe, J. C. Gilloteaux, P. Bozonnet, Y. Creff, and P. Tona. Latching control strategies for a heaving buoy wave energy generator in a random sea. volume 19, 2014. doi:10.3182/20140824-6-za-1003.00440.

[58] Enrico Anderlini. Control of wave energy converters using machine learning strategies. 2018.

[59] J. C.C. Henriques, J. C.C. Portillo, W. Sheng, L. M.C. Gato, and A. F.O. Falcão. Dynamics and control of air turbines in oscillating-water-column wave energy converters: Analyses and case study. *Renewable and Sustainable Energy Reviews*, 112, 2019. doi:10.1016/j.rser.2019.05.010.

[60] Karl J. Astrom and Tore HÄgglund. Advanced pid control, 2006. doi:10.1109/MCS.2006.1580160.

[61] Arthur Pecher, Jens Peter Kofoed, Matt Folley, Ronan Costello, Jørgen Hals Todalshaug, Lars Bergdahl, Amélie Têtu, and Marco Alves. *Ocean Engineering & Oceanography 7: Handbook of ocean wave energy*, volume 7. 2017.

Appendix A

Appendix

Matlab Code

```
%Initialize OWC System Variables

    load ('C:\Users\alves\Desktop\TESE\OWC\Data005.mat')
    load ('C:\Users\alves\Desktop\TESE\OWC\Data004.mat')
    load ('C:\Users\alves\Desktop\TESE\OWC\vars_OWC_IH.mat')

    P_atm = 1.01325 * 10^5;  %[Pascal]
    heat_ratio = 1.4;
    seaWater_rho = 1025; % [kg m^(-3)]
    air_rho = 1.201; % [kg m^(-3)]
    g = 9.81;           % [m s^(-2)]
    piston_width = 4.3; % [m]
    piston_lenght = 10; % [m]
    piston_A = piston_width*piston_lenght;  % free space area  [m^2]
    piston_z =  0; % piston initial position [m]
    piston_w = 0; % piston initial velocity [m/s]
    mtotal = m_piston + A_inf; %  imaginary piston mass + added mass at infinite
    frequency[kg]

    chamber_Vo = piston_A*h_0;    % initial chamber volume[m^3]
    chamber_Vc = chamber_Vo;
    chamber_P = P_atm; %initial chamber pressure [Pascal]
    chamber_Pr = chamber_P / P_atm - 1;  % initial relative pressure in chamber

    turbine_D = 0.5; % turbine diameter

    a = 1*10^(-3); % control parameters a and b
    b = 3;

    Pg_rated = 30*10^3; %rated power [W]
    turbine_speed_nominal = 1470; % turbine nomimal speed [RPM]
    Torque_max = 60*Pg_rated /(2*pi*turbine_speed_nominal); %Maximum torque [NâŃĚm]
```

```
    turbine_speed_threshold = 2^(-1/b)*200; %turbine speed threshold [RPM]

    psi_bep = 0.335;
    pi_bep = 0.0251;

    pressure_head1 = Data004(:,1);
    turbine_flow_rate = Data004(:,2);
    pressure_head2 = Data005(:,1);
    turbine_power = Data005(:,2);

    turbine_inicial_speed = 100; %turbine initial speed [RPM]

    inertia = 5.01; %[kgâŃĚm2]

    dt = 0.001; % simulation time step [s]
    tfinal = 1500;
    t = [0: dt: tfinal]; % time vector [w]

    H1 = JONSWAP(2*pi*freq, 12.5, 1.48);

    Fexc = sum(H1.*Fex*cos(2*pi*freq*t + ph + (-pi + rand(56,1)*(pi+pi)))); %
    Excitation Force [N]

    figure(1)
    plot(t, Fexc)

    function [H] = JONSWAP(w,Tp,Hs)
      nw=length(w);
        gamma=3.3;
      As = 0.0624/(0.230 + (0.0336*gamma) -(0.185/(1.9+gamma)));
      wp=2*pi/Tp;
      H=zeros(1,nw);
      S=zeros(1,nw);
      %stepw = w(2)-w(1);
      stepw = (w(nw) - w(1))/(nw-1);
      for i = 1:nw
          if w(i) < wp
              sigma = 0.07;
          else
              sigma = 0.09;
          end
        Bs = exp(-((w(i) - wp)^2)/(2*sigma^2*wp^2));
        S(i) = As*(Hs^2)*(wp^4)*(w(i)^-5)*gamma^Bs*exp((-5/4)*(wp/w(i))^4);
        H(i) = sqrt(2*S(i)*stepw);
      end
    end
```

Listing A.1: Script to Initialize OWC System Variables

```
%extract data from simulation for training neural network
```

```
count = 1;

for i = .1*10^-3 : .1*10^-3 : 2*10^-3
   a = i;
   for j = 2.5 : 0.1 : 3.2
      b = j;
      result(count).a = a;
      result(count).b = b;
      yout = sim('NeuralNetworkTrainingDataExtract');
      PGen_avg =  yout.PGen_avg.signals.values;
      result(count).avgPwr = PGen_avg(end);
      z = yout.Z.signals.values;
      result(count).zMax = max(z);
      count = count + 1;
   end
end
```

Listing A.2: Script to extract data from simulation for training neural network

```
%Uses a PSO algoritmn to find the the optimal turbine parameters using a neural
    network
global positionLimit Hs Te;
Nparticles = 40;

nparameters = 2;

c1 = 2.6;
c2 = 1.3;
w = 0.9;  %should  be between [0.9;1.2]

positionLimit = [3.7*10^-3 1*10^-4; 3.3 2.5]; %column (parameters), line (max,min)

Hs = 0.88;
Te = 5.5;

particle = PSO(Nparticles,nparameters,c1,c2,w,positionLimit);

%inicializes random values for the position and velocity
function particle = inicialize(Nparticles,nparameters)
  global positionLimit Hs Te;

  for i=1 : Nparticles
    for j=1 : nparameters
       particle(i).x(j) = (positionLimit(j,2) - positionLimit(j,1)) * rand(1,1) +
    positionLimit(j,1);
    end
    particle(i).v = [2*10^-3 3]*rand(1);
    particle(i).pb = particle(i).x;
  end
end
```

```
30
31 %calculates the output value of the fitness function
32 function outputfunction = fitnessfunction(position)
33     global positionLimit Hs Te;
34
35     %calculates average generated power
36     outputPowerAvg = pyrunfile("PredictTurbineParameters.py", "Pavg", a=position(1)
       , b=position(2), Hs=Hs, Te=Te);
37     outputfunction = double(outputPowerAvg);
38
39 end
40
41 function outputvector = outputvectorInicialize(Nparticles,particle)
42   for i=1 : Nparticles
43     outputvector(i,1) = fitnessfunction(particle(i).x);
44     outputvector(i,2) = outputvector(i,1);
45   end
46 end
47
48 %updates personalbest and current value of the output
49 function outputvector = updateOutputVector(Nparticles,outputvector,particle)
50   for i=1 : Nparticles
51     outputvector(i,1) = fitnessfunction(particle(i).x);
52 %     if(outputvector(i,1) > outputvector(i,2))
53 %       outputvector(i,2) = outputvector(i,1);
54 %     end
55   end
56 end
57
58 function outputvector = updateOutputVectorPb(Nparticles,outputvector,particle)
59   for i=1 : Nparticles
60
61     if(outputvector(i,1) > outputvector(i,2))
62       outputvector(i,2) = outputvector(i,1);
63     end
64
65   end
66 % ##  arrayParticleAndOutput = [particle outputvector];
67 end
68
69 %updates the personal best of each particle
70 function particle = personalBest(particle,Nparticles,outputvector)
71   for i=1 : Nparticles
72     if( outputvector(i,2) < outputvector(i,1))
73       particle(i).pb = particle(i).x;
74     end
75   end
76 end
77
```

```
78 %updates the global best
79 function globalbest = globalBest(particle,Nparticles,outputvector)
80
81   maxvalue = -1E99;
82   position = 0;
83
84   for i=1 : Nparticles
85     if(maxvalue < outputvector(i,2))
86       maxvalue = outputvector(i,2);
87       position = i;
88     end
89   end
90
91   globalbest = particle(position).pb;
92
93 end
94
95 %updates the velocity of each particle parameter
96 function particle = updateVelocity(particle,Nparticles,nparameters,c1,c2,w,
       globalbest)
97
98   for i=1 : Nparticles
99     for j=1 : nparameters
100      particle(i).v(j) = w*particle(i).v(j) + c1*rand(1)*(particle(i).pb(j) -
       particle(i).x(j)) + c2*rand(1)*(globalbest(j) - particle(i).x(j));
101    end
102  end
103
104 end
105
106 %updates the position of each particle parameter
107 function particle = updatePosition(particle,Nparticles,nparameters,positionLimit)
108
109   for i=1 : Nparticles
110     for j=1 : nparameters
111       particle(i).x(j) = particle(i).x(j) + particle(i).v(j);
112       if(particle(i).x(j) > positionLimit(j,1))
113         particle(i).x(j) = positionLimit(j,1);
114         particle(i).v(j) = 0;
115       elseif(particle(i).x(j) < positionLimit(j,2))
116         particle(i).x(j) = positionLimit(j,2);
117         particle(i).v(j) = 0;
118       end
119     end
120   end
121
122 end
123
124 function weights = updateWeights(c1,c2,w,i)
```

```
  c1 = max(-0.22*i + 2.6, 0.2);
  c2 = max(-0.11*i + 1.3, 0.4);
  w = max(-0.008*i + 0.9, 0.1);

  weights = [c1; c2; w];

end

function globalbest = PSO(Nparticles,nparameters,c1,c2,w,positionLimit)
  particle = inicialize(Nparticles,nparameters);
  outputvector = outputvectorInicialize(Nparticles,particle);
  matrix = cell2mat(struct2cell(particle));
  globalbest = globalBest(particle,Nparticles,outputvector);
  i=0;
  while(i < 25)
    outputvector = updateOutputVector(Nparticles,outputvector,particle);
    particle = personalBest(particle,Nparticles,outputvector);
    outputvector = updateOutputVectorPb(Nparticles,outputvector,particle);
    globalbest = globalBest(particle,Nparticles,outputvector);

    weights = updateWeights(c1,c2,w,i);

    c1 = weights(1);
    c2 = weights(2);
    w = weights(3);

    particle = updateVelocity(particle,Nparticles,nparameters,c1,c2,w,globalbest);
    particle = updatePosition(particle,Nparticles,nparameters,positionLimit);


    i = i + 1;
  end
end
```

Listing A.3: Script with a PSO algoritmn to find the the optimal turbine parameters using a neural network

```
%PID tuner using a PSO with a IAE
global positionLimit;
Nparticles = 40;

nparameters = 4;

c1 = 2.6;
c2 = 1.3;
w = 0.9;  %should  be between [0.9;1.2]

positionLimit = [50 -50; 50 -50; 50 -50; 100 0.1]; %column (parameters), line (max,
    min)

```

```
particle = PSO(Nparticles,nparameters,c1,c2,w,positionLimit);


%inicializes random values for the position and velocity
function particle = inicialize(Nparticles,nparameters)
  global positionLimit;

  for i=1 : Nparticles
    for j=1 : nparameters
       particle(i).x(j) = (positionLimit(j,2) - positionLimit(j,1)) * rand(1,1) +
    positionLimit(j,1);
    end
    particle(i).v = 2*rand(1,nparameters);
    particle(i).pb = particle(i).x;
  end

end

%calculates the output value of the fitness function, setting PID parameters
function outputfunction = fitnessfunction(position)

    Ti = position(1)/position(2);
    Td = position(3)/position(1);
    kd = (Ti+Td)/2;
    %calculates average generated power
    p_sprint = sprintf('%f', position(1));
    i_sprint = sprintf('%f', position(2));
    d_sprint = sprintf('%f', position(3));
    n_sprint = sprintf('%f', position(4));
    kd_sprint = sprintf('%f', kd);
    set_param('PID_Correct/Subsystem1/PID_control', 'P', p_sprint);
    set_param('PID_Correct/Subsystem1/PID_control', 'I', i_sprint);
    set_param('PID_Correct/Subsystem1/PID_control', 'D', d_sprint);
    set_param('PID_Correct/Subsystem1/PID_control', 'N', n_sprint);
    set_param('PID_Correct/Subsystem1/PID_control', 'Kb', kd_sprint);
    yout = sim('PID_Correct');
    error =  yout.error.signals.values;
    absolute_mean_error = error(end);
    IAE = absolute_mean_error*1000;
    outputfunction = 1/IAE;
end

function outputvector = outputvectorInicialize(Nparticles,particle)

  for i=1 : Nparticles
    outputvector(i,1) = fitnessfunction(particle(i).x);
    outputvector(i,2) = outputvector(i,1);
  end
end
```

```
61
62 %updates personalbest and current value of the output
63 function outputvector = updateOutputVector(Nparticles,outputvector,particle)
64   for i=1 : Nparticles
65     outputvector(i,1) = fitnessfunction(particle(i).x);
66 %      if(outputvector(i,1) > outputvector(i,2))
67 %        outputvector(i,2) = outputvector(i,1);
68 %      end
69   end
70 end
71
72 function outputvector = updateOutputVectorPb(Nparticles,outputvector,particle)
73   for i=1 : Nparticles
74
75     if(outputvector(i,1) > outputvector(i,2))
76       outputvector(i,2) = outputvector(i,1);
77     end
78
79   end
80 % ##  arrayParticleAndOutput = [particle outputvector];
81 end
82
83 %updates the personal best of each particle
84 function particle = personalBest(particle,Nparticles,outputvector)
85   for i=1 : Nparticles
86     if( outputvector(i,2) < outputvector(i,1))
87       particle(i).pb = particle(i).x;
88     end
89   end
90 end
91
92 %updates the global best
93 function globalbest = globalBest(particle,Nparticles,outputvector)
94
95   maxvalue = -1E99;
96   position = 0;
97
98   for i=1 : Nparticles
99     if(maxvalue < outputvector(i,2))
100      maxvalue = outputvector(i,2);
101      position = i;
102    end
103  end
104
105  globalbest = particle(position).pb;
106
107 end
108
109 %updates the velocity of each particle parameter
```

```
110 function particle = updateVelocity(particle,Nparticles,nparameters,c1,c2,w,
        globalbest)
111
112   for i=1 : Nparticles
113     for j=1 : nparameters
114       particle(i).v(j) = w*particle(i).v(   j) + c1*rand(1)*(particle(i).pb(j) -
        particle(i).x(j)) + c2*rand(1)*(globalbest(j) - particle(i).x(j));
115     end
116   end
117
118 end
119
120 %updates the position of each particle parameter
121 function particle = updatePosition(particle,Nparticles,nparameters,positionLimit)
122
123   for i=1 : Nparticles
124     for j=1 : nparameters
125       particle(i).x(j) = particle(i).x(j) + particle(i).v(j);
126       if(particle(i).x(j) > positionLimit(j,1))
127         particle(i).x(j) = positionLimit(j,1);
128         particle(i).v(j) = 0;
129       elseif(particle(i).x(j) < positionLimit(j,2))
130         particle(i).x(j) = positionLimit(j,2);
131         particle(i).v(j) = 0;
132       end
133     end
134   end
135
136 end
137
138 function weights = updateWeights(c1,c2,w,i)
139   c1 = max(-0.22*i + 2.6, 0.2);
140   c2 = max(-0.11*i + 1.3, 0.4);
141   w = max(-0.008*i + 0.9, 0.1);
142
143   weights = [c1; c2; w];
144
145 end
146
147 function globalbest = PSO(Nparticles,nparameters,c1,c2,w,positionLimit)
148   particle = inicialize(Nparticles,nparameters);
149   outputvector = outputvectorInicialize(Nparticles,particle);
150   matrix = cell2mat(struct2cell(particle));
151   globalbest = globalBest(particle,Nparticles,outputvector);
152   i=0;
153   while(i < 20)
154
155     outputvector = updateOutputVector(Nparticles,outputvector,particle);
156     particle = personalBest(particle,Nparticles,outputvector);
```

```
    outputvector = updateOutputVectorPb(Nparticles,outputvector,particle);
    globalbest = globalBest(particle,Nparticles,outputvector);

    weights = updateWeights(c1,c2,w,i);

    c1 = weights(1);
    c2 = weights(2);
    w = weights(3);

    particle = updateVelocity(particle,Nparticles,nparameters,c1,c2,w,globalbest);
    particle = updatePosition(particle,Nparticles,nparameters,positionLimit);



    i = i + 1
  end
end
```

Listing A.4: Script of PID tuner using a PSO with a IAE

Python Code

```
import tensorflow as tf
from tensorflow.keras.models import Sequential
from tensorflow.keras.layers import Input, Dense, Dropout

def get_models_layer(num_layers:int,
                min_nodes_per_layer:int,
                max_nodes_per_layer:int,
                node_step_size:int,
                input_shape: tuple,
                hidden_layer_activation: str = 'relu',
                num_nodes_at_output: int = 1,
                 ) -> list:

    node_options = list(range(min_nodes_per_layer, max_nodes_per_layer+1,
    node_step_size))
    layer_possibilities = [node_options] * num_layers
    layer_node_permutations = list(itertools.product(*layer_possibilities))

    models = []
    for permutation in layer_node_permutations:
        model = tf.keras.Sequential()
        model.add(tf.keras.layers.InputLayer(input_shape=input_shape))
        model_name = ''

        for nodes_at_layers in permutation:
            model.add(tf.keras.layers.Dense(nodes_at_layers,activation =
    hidden_layer_activation))
            model_name += f'dense{nodes_at_layers}_'
```

```

        model.add(tf.keras.layers.Dense(num_nodes_at_output))
        model._name = model_name[:-1]

        models.append(model)

    return models



def get_all_models(min_number_layer:int,
                   max_number_layer:int) -> list:
    all_models = []

    for x in range(min_number_layer, max_number_layer):
        all_models = get_models_layer(num_layers = x,min_nodes_per_layer = 16,
    max_nodes_per_layer = 256,node_step_size = 16,input_shape = (4,))
        all_models.append(all_models)

    return all_models
```

Listing A.5: Scrips to create all different architecture to further test

```

def optimize(models: list,
             X_train: np.array,
             y_train: np.array,
             X_test: np.array,
             y_test: np.array,
             epochs: int = 100,
             verbose: int = 0) -> pd.DataFrame:

    results = []

    def train(model: tf.keras.Sequential) -> dict:
        model.compile(
            loss = tf.keras.losses.mae,
            optimizer=tf.keras.optimizers.RMSprop(),
            metrics=[tf.keras.metrics.BinaryAccuracy(name='MeanAbsoluteError')]
        )
        model.fit(X_train, y_train, epochs=epochs, verbose=verbose, validation_data
    =(X_test,y_test))

        # Make predictions on the test set
        preds = model.predict(X_test)

        # Return evaluation metrics on the test set
        return {
            'model_name': model.name,
            'mae': mean_absolute_error(y_test, preds),
```

```
        }

    for model in models:
        try:
            print(model, end = '...')
            res = train(model=model)
            results.append(res)
        except Exception as e:
            print(f'{model.name} --> {str(e)}')

    return pd.DataFrame(results)
```

Listing A.6: Script to train all models